Geophysical Journal International

Geophys. J. Int. (2013) **194,** 249–268
Advance Access publication 2013 April 24

doi: 10.1093/gji/ggt120

3-D Cauchy-type integrals for terrain correction of gravity and gravity gradiometry data

Michael S. Zhdanov[1,2] and Xiaojun Liu[2]

[1] *TechnoImaging,* 4001 *South,* 700 *East, Suite* 500, *Salt Lake City, UT* 84107, *USA. E-mail: michael.s.zhdanov@gmail.com*
[2] *Department of Geology and Geophysics, University of Utah,* 115 *South,* 1460 *East, Room* 383, *Salt Lake City, UT* 84112, *USA*

Accepted 2013 March 25. Received 2013 March 23; in original form 2012 September 16

SUMMARY

Fundamental to complex analysis is the Cauchy integral theorem, and the derivation of Cauchy-type integrals. For over 40 yr, Cauchy-type integrals have been used to describe analytical continuation, establish the location of singular points, and study non-single-valued solutions of inverse problems in 2-D potential field theory. In this paper, we revive this interesting and fundamental area of potential field theory to introduce Cauchy-type integrals for 3-D potential fields. In particular, we show how one can evaluate the gravity and gravity gradiometry responses of 3-D bodies as surface integrals over arbitrary volumes that may contain spatially variable densities. This method of 3-D spatial-domain potential field modelling has never been realized before, and we show how it is particularly suited to the terrain correction of airborne gravity and gravity gradiometry data. The surface integrals are evaluated numerically on a topographically conforming grid with a resolution equal to the digital elevation model. Thus, our method directly avoids issues related to prismatic discretization of the digital elevation model and their associated volume integration which may result in inappropriate discretization of the earth model, particularly for regions of rugged topography. We demonstrate our method with a model study for airborne gravity gradiometry data simulated for a next-generation 1 Eö/$\sqrt{\text{Hz}}$ system over the Kauring test site in Western Australia.

Key words: Gravity anomalies and Earth structure; Geopotential theory.

1 INTRODUCTION

The Cauchy integral theorem and Cauchy-type integrals are of significant importance to 2-D potential field theory, as they are used to describe analytical continuation of potential fields, establish the location of their singular points, and study non-single-valued solutions of their inverse problems. It was shown in the works of Zhdanov (1973, 1974, 1975, 1980) that logarithmic potential theory can be extended to the 3-D case by constructing Cauchy-type integral analogues for 3-D potential fields, based on ideas originally introduced by Moisil & Theodoresco (1931) and Bitsadze (1953, 1972). This theory was consolidated and significantly expanded by Zhdanov (1984, 1988). Unfortunately, this interesting and fundamental area of potential field theory has since been dormant. In this paper, we revive the study of 3-D Cauchy-type integrals for potential fields. This paper is very thorough in the way it introduces a rigorous representation of the gravity field and its gradients in terms of 3-D Cauchy-type integrals. In particular, we realize an entirely new method for 3-D spatial-domain modelling of gravity gradient fields as surface integrals over arbitrary volumes that may have spatially variable densities.

Our first application of 3-D Cauchy-type integrals is for improved terrain (including bathymetry) correction of gravity and gravity gradiometry data whereby we evaluate the gravity and gravity gradient responses as surface integrals over the surface of the elevation (bathymetry) model. This surface integration ensures accurate representation of the terrain (bathymetry) response. For this purpose we use triangular discretization of the density contrast surface in computing the Cauchy-type integrals over this surface. This triangular discretization is similar to one used by Hammer *et al.* (1991), who applied the so called seminorm minimization of Parker *et al.* (1987) for gravity inversion to model the density structure of discrete bodies using the body shape and a plane of gravity data as the only inputs. Our approach is different because it directly employs the analytical properties of the 3-D Cauchy-type integrals resulting at surface integrals over the contrast surface only with arbitrary spatially variable densities below the contrast surface. Note also that, Hammer *et al.* (1991) do not use the surface integral per se; their integral representation requires additional numerical evaluation of some auxiliary elliptical integrals. At the same time, the 3-D Cauchy-type surface integrals over the contrast surface, introduced in our paper, do not require any elliptical integral calculations.

Terrain corrections are a means of reducing the dynamic range in gravity and gravity gradiometry data so as to reveal the more subtle geological responses present. There are a number of factors that influence the validity of terrain corrections, including the accuracy of the aircraft position, resolution of the digital

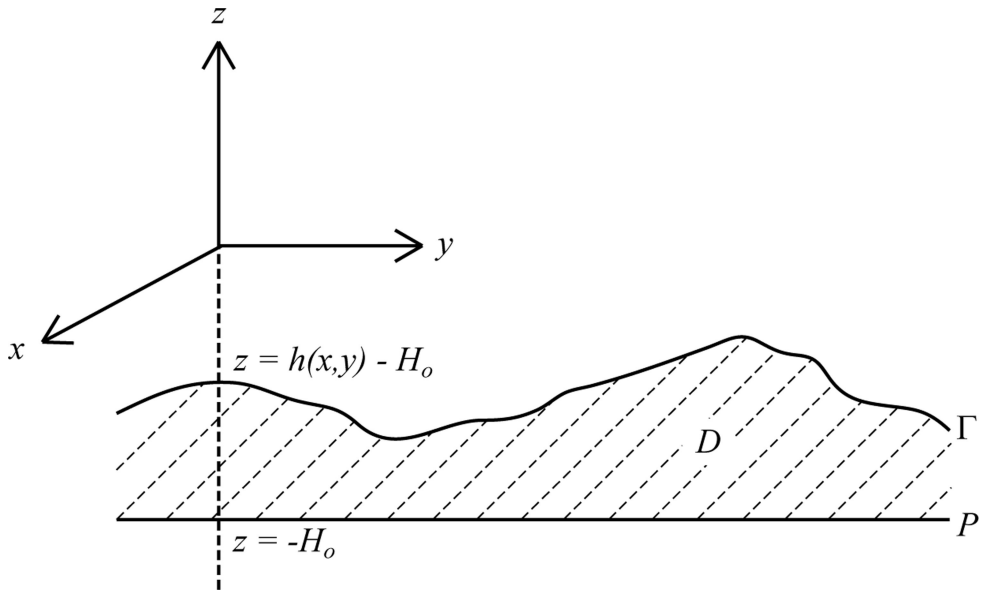

Figure 1. Schematic of the 3-D terrain model D, contained within a surface Γ described by the function $h(x, y)$, and a lower plane P.

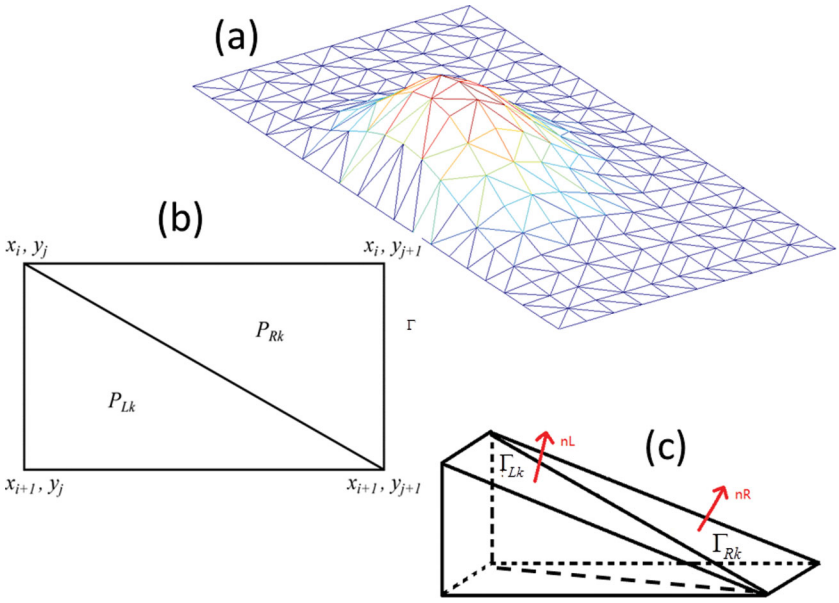

Figure 2. Triangular discretization of the density contrast surface: (a) schematic view of triangular mesh grid; (b) each rectangular cell of the mesh $\sum$ is divided into two triangulars, which form the elementary cells P_{Lk} (left triangular) and P_{Lk} (right triangular); (c) 3-D view of two neighboured prisms with triangulated tops, Γ_{Lk} and Γ_{Rk}.

elevation model (DEM), the way the terrain is approximated, and the methods used to filter the predicted responses to match the instrument's acquisition system and post-acquisition processing. These factors are particularly important for terrain corrections to sub-Eö levels, particularly as the next generation of 1 Eö/$\sqrt{\text{Hz}}$ airborne gravity gradiometers are now being developed and tested.

Terrain corrections are generally calculated as the response due to the volume of earth bound by an upper surface of the digital elevation model (DEM) and a lower surface of a plane that passes through the lowest elevation of the survey area. For airborne gravity gradiometry (AGG) at low survey heights and where there are large variations in topographic relief, a high resolution DEM is required. For existing AGG instruments, the DEM needs to be sampled at a resolution approximately one-third to one-half of the flight height, and have a vertical accuracy better than 1 m (Dransfield & Zeng 2009). For these accuracies, LIDAR data are routinely measured with resolution of the order of 1 m and sub-metre vertical accuracy. Yet, LiDAR only provides the DEM in a swathe under each flight line. At low flight heights and with wide line spacing, gaps in the LiDAR-based DEM may exist between the flight lines. Also, over those areas flown at a flight height greater than the laser range and over water surfaces with poor dispersion, there will be gaps in the LiDAR-based DEM. Moreover, for quality terrain correction, DEM data from beyond the survey area (typically up to 10 km) are required. For this reason, LiDAR-based DEMs are usually merged with other DEMs, for example, shuttle radar topography mission (SRTM) data measured circa 90 m resolution. Although SRTM data is inadequate for terrain corrections directly beneath the aircraft, it is sufficiently accurate for terrain corrections at greater distance from the aircraft, such as between lines or outside the survey area.

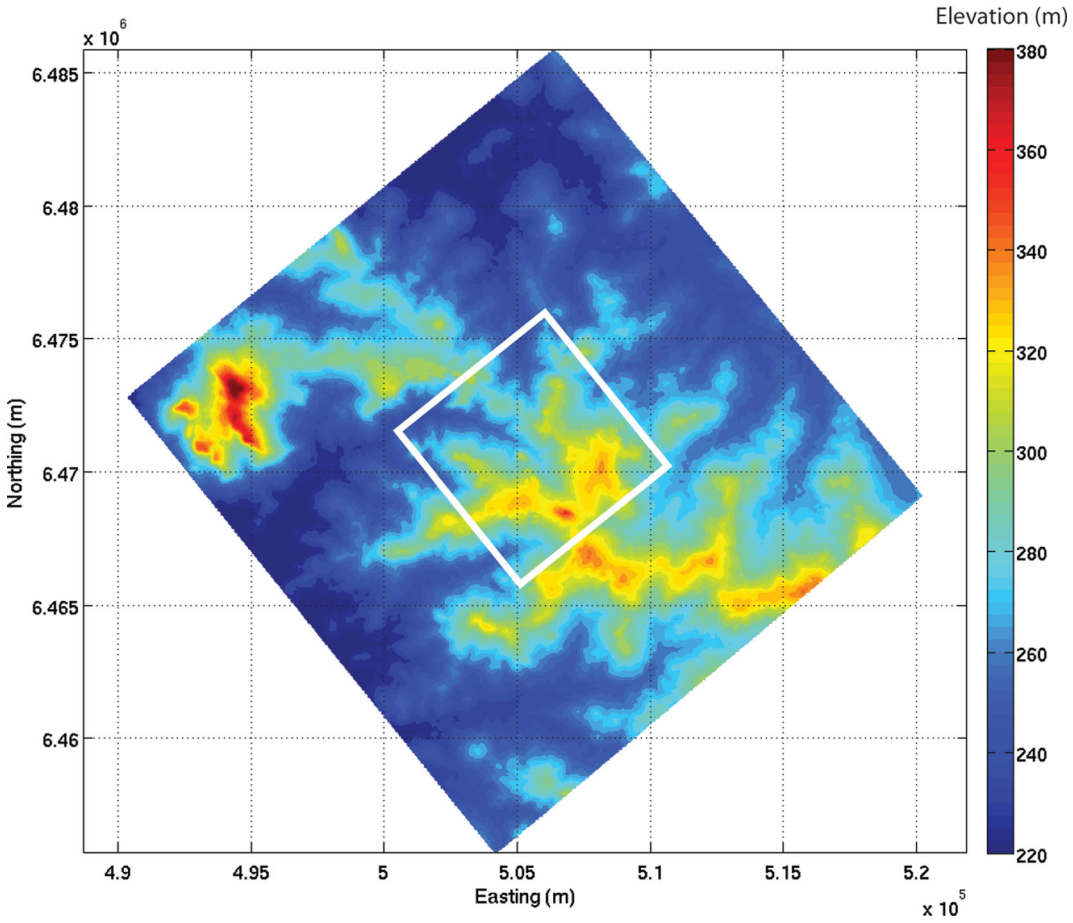

Figure 3. Digital elevation model over the Kauring test site used for terrain correction using the 3-D Cauchy-type integral method. The area within the white square was measured from a 10 m resolution LiDAR survey. The area outside the white square was obtained from the SRTM database.

Water surfaces are usually treated as flat surfaces mapped from the traced shorelines.

It is standard practice that the volume beneath the merged DEM is discretized into a grid of right rectangular prisms of heights representative of the terrain. These prisms are usually assigned a constant density of 1 g cm^{-3}. This particular spatial domain method is quite inefficient (e.g. Hwang *et al.* 2003; Jekeli & Zhu 2006). Computations can be reduced by recognizing that high resolution DEMs are required for terrain corrections where there are large variations in topographic relief, and this resolution can be relaxed as the distance from the observation point is increased. It follows that most extant workflows perform modelling with prescribed or quadtree coarsing of the terrain as the distance from the observation point is increased (e.g. Dransfield & Zeng 2009; Davis *et al.* 2011). Alternative methods of 3-D modelling are based on FFT-based wavenumber domain methods, such as those of Parker (1973, 1995, 1996).

Measured free-air data are also filtered by the acquisition system and during post-acquisition processing. We should note that filtering of airborne data has a large effect on values of terrain corrections. For example, Fugro Airborne Surveys' fixed-wing FALCON system's various filtering processes have been emulated with a sixth- or seventh-order Butterworth filter of 0.18 Hz cut-off frequency (approximately 300 m) in the direction of the flight lines (e.g. Lane 2004; Dransfield & Zeng 2009). Bell Geospace's method of full tensor noise reduction (FTNR) requires a cut-off wavelength that is usually set at the line spacing, meaning that Air-FTG data have the appearance of being filtered where the width of the filter is purely that of the line spacing (e.g. Murphy 2010). As the higher frequencies have mostly been removed in the acquired and processed data, the terrain correction also needs to be filtered in the same manner to avoid adding in higher frequency terrain content (Kass & Li 2008). The filtered 1 g cm^{-3} terrain corrections then allows the use of any desired terrain density, which is usually between 2.4 and 3.1 g cm^{-3} and is chosen to be most representative of the host geology. Often, the average crustal density of 2.67 g cm^{-3} is used. The terrain corrected data are obtained by subtracting the product of the terrain density and the terrain correction from the free-air data.

We should note also that, in this paper we consider the planar approximation for terrain correction, which is usually used in geophysical applications. However, the mathematical method, developed in our paper, is general and can be used for geodetic applications with ellipsoidal geometry of the earth, as well. However, this will be a subject of a separate paper.

2 3-D CAUCHY-TYPE INTEGRALS AND THEIR PROPERTIES

A thorough description of 3-D Cauchy-type integrals was presented in the monographs by Zhdanov (1984, 1988). However, since those monographs are not readily accessible to the wider geophysics community, we commence this paper with an introduction to 3-D Cauchy-type integrals.

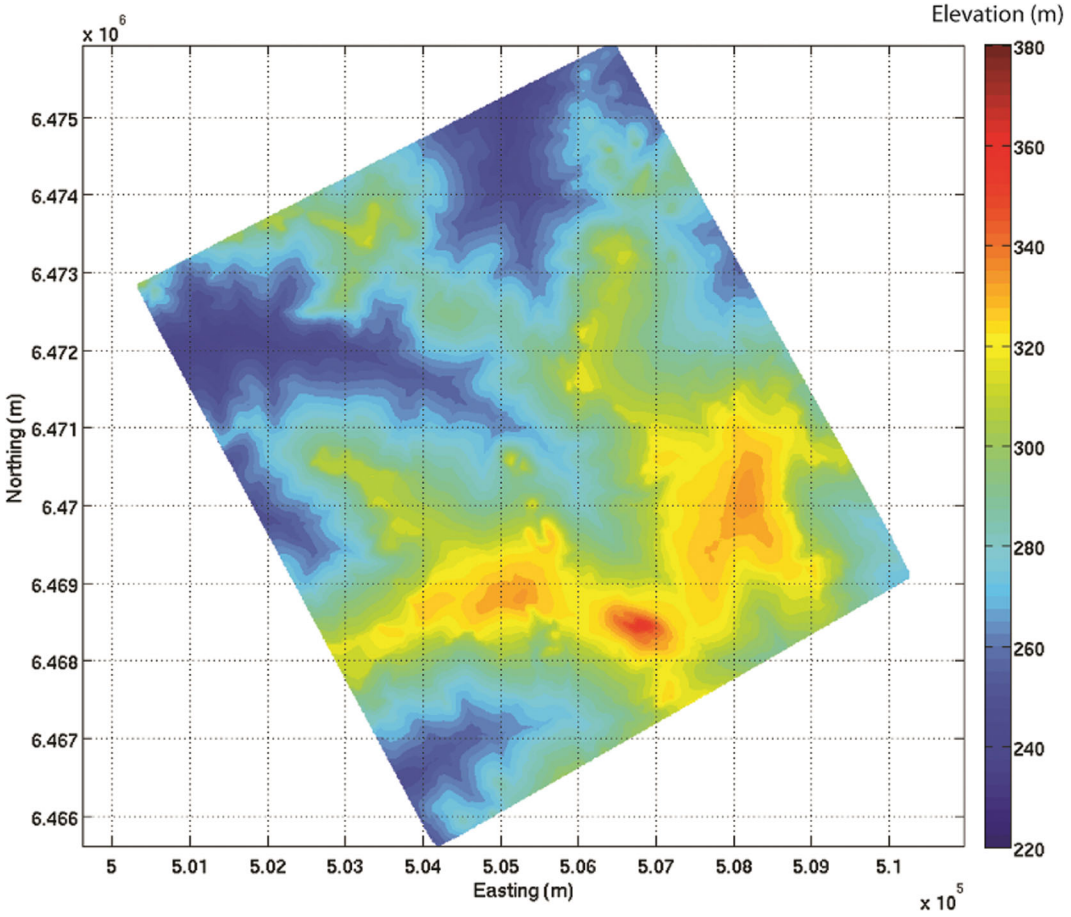

Figure 4. Digital elevation model over the Kauring test site as measured from a 10 m resolution LiDAR survey.

Following Zhdanov (1984, 1988), the 3-D Cauchy-type integral is represented by the following expression

$$\mathbf{C}^S\left(\mathbf{r}',\varphi\right) = -\frac{1}{4\pi}\iint_S\left[(\mathbf{n}\cdot\varphi)\nabla\frac{1}{|\mathbf{r}-\mathbf{r}'|}+(\mathbf{n}\times\varphi)\right.$$
$$\left.\times\nabla\frac{1}{|\mathbf{r}-\mathbf{r}'|}\right]ds, \qquad (1)$$

where S is some closed surface, $\varphi=\varphi(\mathbf{r})$ is some vector function specified on S and continuous on S, and $\mathbf{n}$ is a unit vector of the normal to S directed outside the domain D, bounded by the surface S. Function φ is called a vector density of the Cauchy-type integral $\mathbf{C}^S(\mathbf{r}',\varphi)$. It was shown by Zhdanov (1984, 1988) that everywhere outside S, the vector function $\mathbf{C}^S$ satisfies the following equations:

$$\nabla'\cdot\mathbf{C}^S\left(\mathbf{r}',\varphi\right)=0,\quad \nabla'\times\mathbf{C}^S\left(\mathbf{r}',\varphi\right)=0, \qquad (2)$$

where prime denotes a differentiation with respect to vector variable $\mathbf{r}'$. Therefore, vector field $\mathbf{C}^S(\mathbf{r}',\varphi)$ is harmonic and its scalar components are harmonic functions everywhere outside the surface S. In the special case where $\varphi(\mathbf{r})$ represents the boundary values on S of the gradient of a function harmonic inside domain D, we have the following Cauchy integral equation

$$\mathbf{C}^S\left(\mathbf{r}',\varphi\right)=\begin{cases}\varphi\left(\mathbf{r}'\right), & \mathbf{r}'\in D\\ \mathbf{0}, & \mathbf{r}'\in CD\end{cases}, \qquad (3)$$

where CD is an infinite domain complementing the closed domain, $\overline{D}=D+S$, with respect to the whole space. The remarkable property of the 3-D Cauchy-type integral is that in 2-D case, eq. (1) is reduced to the classical Cauchy integral from complex analysis.

One important equation from complex analysis is the Pompei equation, which solves the boundary value problem for arbitrary functions of the complex variable (e.g. Gakhov 1997). Following Zhdanov (1984, 1988) and Davies *et al.* (1989), one can formulate an important 3-D analog of Pompei formula for a potential field, **F**,

Table 1. Specifications of the synthetic targets in the Kauring synthetic model.

Target	Depth to top (m)	Density contrast (g cm^{-3})	Comments
1	500	0.20	Tabular block (e.g. intrusive dike)
2	0	0.15	Dipping sheet (e.g. intrusive dyke)
3	50	0.30	Sphere (e.g. nickel sulphide)
4	150	−0.40	Truncated cone (e.g. kimberlite)
5	3	−2.70	Tabular block (e.g. tunnel)

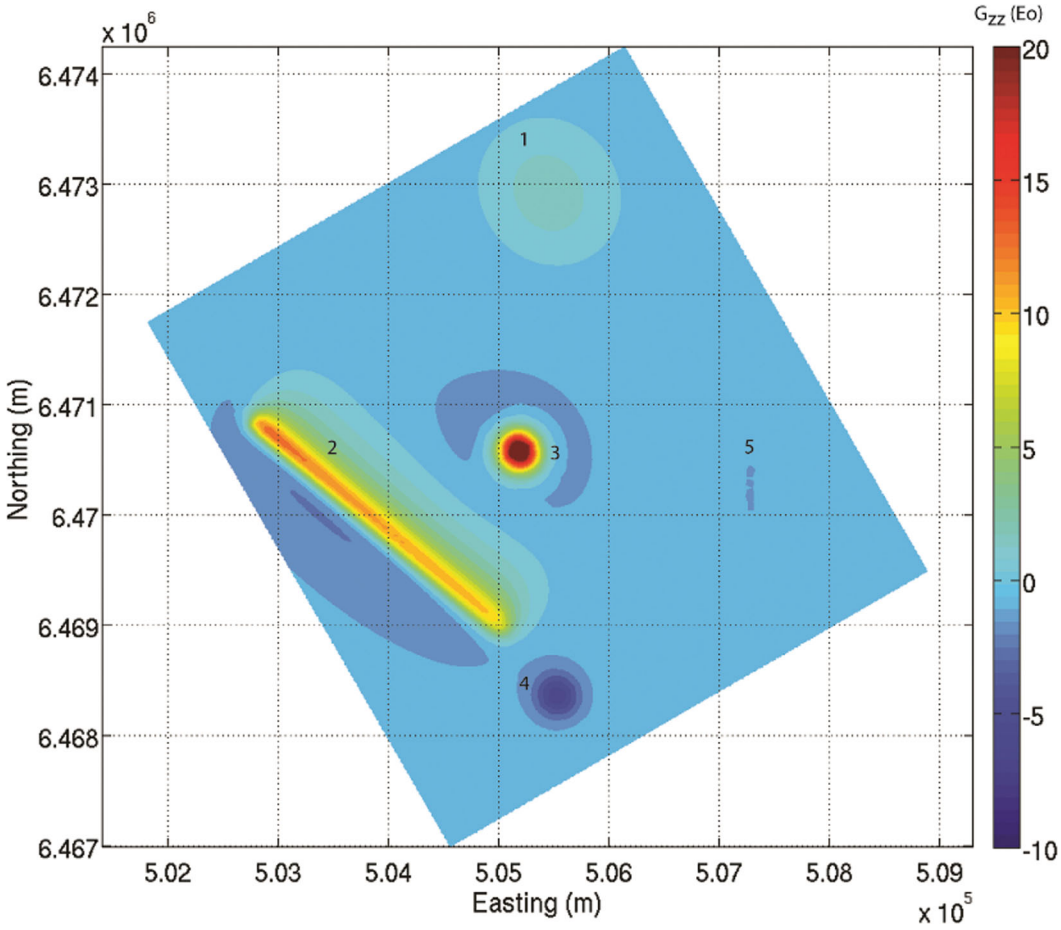

Figure 5. Synthetic, noise-free G_{zz} data calculated by RTX using *ModelVision* with no terrain effect. Each of the targets are identified by their corresponding number in Table 1.

defined within a domain, D

$$\mathbf{C}^S\left(\mathbf{r}', \mathbf{F}\right) + \frac{1}{4\pi}\iiint_D (\nabla\cdot\mathbf{F})\nabla\frac{1}{|\mathbf{r}-\mathbf{r}'|}dv = \begin{cases}\mathbf{F}(\mathbf{r}'), & \mathbf{r}'\in D\\ \mathbf{0}, & \mathbf{r}'\in CD\end{cases}, \tag{4}$$

where the vector field, $\mathbf{F}$, satisfies the equation:

$$\nabla\times\mathbf{F}=0,\ \mathbf{r}\in D. \tag{5}$$

The derivation of the Pompei formula (4) is based on the Gauss theorem, and it is given in Appendix A. 3-D Pompei formula provides a solution of the boundary-value problem for an arbitrary potential field. If the vector field, $\mathbf{F}$, is a Laplacian field in D, that is, $\nabla\times\mathbf{F}=0$, $\nabla\cdot\mathbf{F}=0$, eq. (4) directly yields the 3-D Cauchy-type integral eq. (3).

In this paper, we introduce the method of the Cauchy surface integral to calculate the gravity and gravity gradient fields of 3-D mass distributions. In subsequent sections, the equations are based on a matrix representation of the vector eq. (4). We introduce some Cartesian system of coordinates with the basis $\{\mathbf{d}_x, \mathbf{d}_y, \mathbf{d}_z\}$, where the z axis is directed upward. In this case, the vector form of Cauchy-type integral $\mathbf{C}^S(\mathbf{r}', \varphi)$ can be written in matrix notation using the scalar components of the corresponding vectors. In particular, we represent the vectors $\mathbf{C}^S$, φ, $\mathbf{n}$ and $\nabla\frac{1}{|\mathbf{r}-\mathbf{r}'|}$ in the Cartesian basis $\{\mathbf{d}_x, \mathbf{d}_y, \mathbf{d}_z\}$ as

$$\mathbf{C}^S = C^S_\alpha\mathbf{d}_\alpha,\ \varphi=\varphi_\beta\mathbf{d}_\beta,\ \mathbf{n}=n_\xi\mathbf{d}_\xi,$$

$$\nabla\frac{1}{|\mathbf{r}-\mathbf{r}'|} = -\frac{\mathbf{r}-\mathbf{r}'}{|\mathbf{r}-\mathbf{r}'|^3} = -\frac{r_\eta - r'_\eta}{|\mathbf{r}-\mathbf{r}'|^3}\mathbf{d}_\eta;$$

$$r_\eta=\eta;\ \ \alpha,\beta,\xi,\eta = x,y,z, \tag{6}$$

where we use an agreement on summation that the twice repeated index indicates the summation over this index. Using these notations, eq. (1) can be written as:

$$C^S_\alpha\left(\mathbf{r}', \varphi\right) = -\frac{1}{4\pi}\iint_S \Delta_{\alpha\beta\xi\eta}\varphi_\beta\frac{r_\eta - r'_\eta}{|\mathbf{r}-\mathbf{r}'|^3}n_\xi ds,$$

$$\alpha,\beta,\xi,\eta = x,y,z, \tag{7}$$

where the four-index Δ-symbol is expressed in the terms of the symmetric Kronecker symbol $\delta_{\alpha\beta}$:

$$\Delta_{\alpha\beta\xi\eta} = \delta_{\alpha\beta}\delta_{\xi\eta} + \delta_{\alpha\eta}\delta_{\beta\xi} - \delta_{\alpha\xi}\delta_{\beta\eta};\ \delta_{\alpha\beta} = \begin{cases}1, & \alpha=\beta,\\ 0, & \alpha\neq\beta.\end{cases} \tag{8}$$

We use the term 'matrix form' of the Cauchy-type integral to distinguish from the 'vector form' given by eq. (1). The reason is that in eq. (7), all vectors and the integral kernel are represented by the scalar components of the corresponding matrices describing these vectors, and all mathematical symbols with indices (e.g. $\Delta_{\alpha\beta\xi\eta}$)

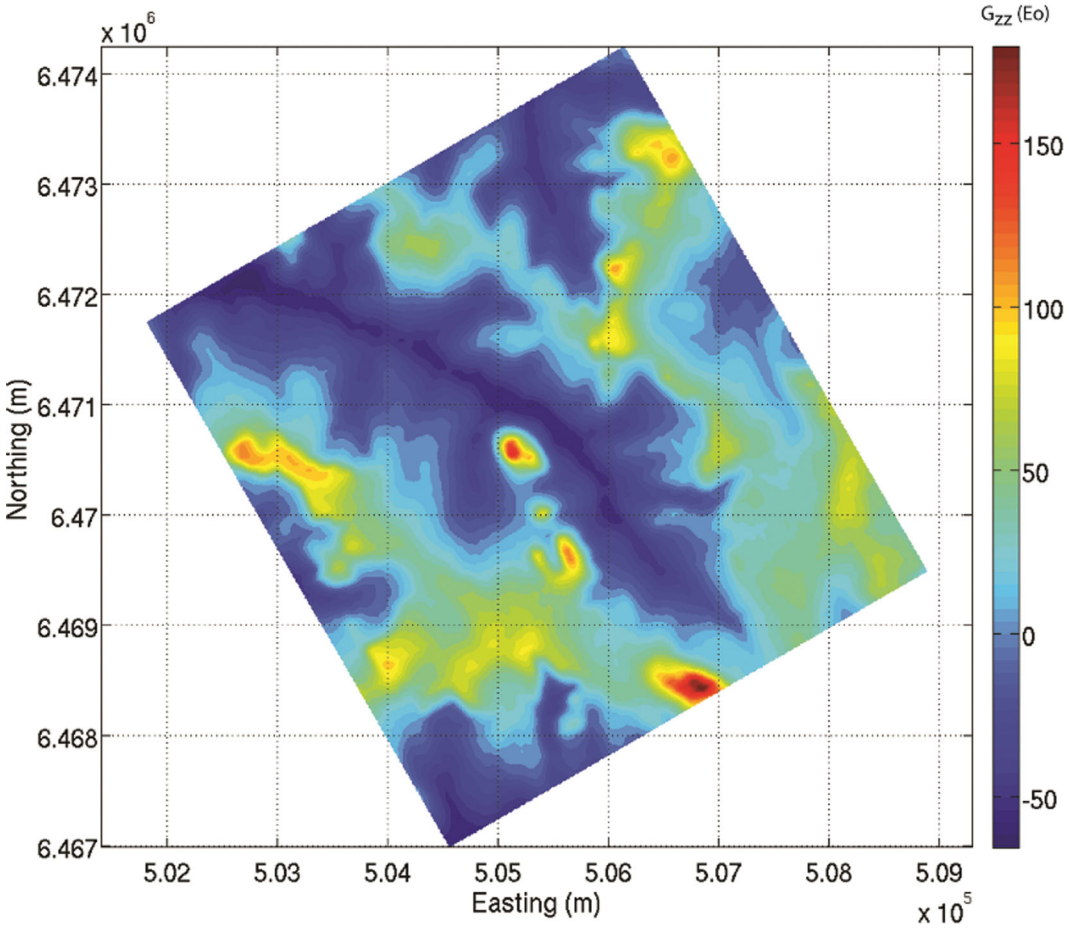

Figure 6. Synthetic free-air G_{zz} data calculated by RTX with terrain effect added, contaminated with noise representative of a 1 Eö/$\sqrt{\text{Hz}}$ (at 1 Hz) instrument.

represent the elements of the corresponding matrices. For completeness, a detailed derivation of the matrix form of the Cauchy-type integral is given in Appendix B.

3 ANALYTICAL FORMS OF THE CAUCHY-TYPE REPRESENTATION OF THE GRAVITY FIELD AND ITS GRADIENTS

3.1 Representing the gravity field in terms of 3-D Cauchy-type integrals

For the sake of simplicity, we begin our analysis with the case where the masses are distributed with a constant density, ρ_0, within some 3-D volume D. Later on we will consider a case of the arbitrary density distribution.

The gravity field $\mathbf{g}(\mathbf{r})$ satisfies the equations:

$$\nabla \cdot \mathbf{g} = -4\pi G\rho_0, \quad \nabla \times \mathbf{g} = 0, \tag{9}$$

where G is the universal gravitational constant. Following Zhdanov (1988), we introduce the auxiliary vector field, $\mathbf{F}$, which has the form:

$$\mathbf{F} = \frac{4\pi}{3} G\rho_0 \mathbf{r}, \text{ and } \nabla \cdot \mathbf{F} = 4\pi G\rho_0. \tag{10}$$

Substituting expressions (10) into the 3-D Pompei eq. (4), we find:

$$\mathbf{C}^S\left(\mathbf{r}', \frac{4\pi}{3} G\rho_0 \mathbf{r}\right) + G\iiint_D \rho_0 \nabla \frac{1}{|\mathbf{r}-\mathbf{r}'|} dv = \begin{cases} \frac{4\pi}{3} G\rho_0 \mathbf{r}', & \mathbf{r}' \in D, \\ \mathbf{0}, & \mathbf{r}' \in CD. \end{cases} \tag{11}$$

The volume integral in the left-hand part of eq. (11) is (with the negative sign) the gravity field $\mathbf{g}(\mathbf{r}')$ of a domain, D:

$$\mathbf{g}\left(\mathbf{r}'\right) = -G\iiint_D \rho_0 \nabla \frac{1}{|\mathbf{r}-\mathbf{r}'|} dv, \tag{12}$$

expressed in the well known form of a volume integral. At the same time, it is useful to express the same gravity field in terms of a surface integral over the same domain, D. Thus, we can arrive at a representation of the gravity field in terms of a 3-D Cauchy-type integral:

$$\mathbf{g}\left(\mathbf{r}'\right) = \begin{cases} -\frac{4\pi}{3} G\rho_0 \mathbf{r}' + \frac{4\pi}{3} G\rho_0 \mathbf{C}^S\left(\mathbf{r}', \mathbf{r}\right), & \mathbf{r}' \in D, \\ \frac{4\pi}{3} G\rho_0 \mathbf{C}^S\left(\mathbf{r}', \mathbf{r}\right), & \mathbf{r}' \in CD. \end{cases} \tag{13}$$

In a case where $\mathbf{r}' \in CD$, we have from eq. (13):

$$\mathbf{g}\left(\mathbf{r}'\right) = \frac{4\pi}{3} G\rho_0 \mathbf{C}^S\left(\mathbf{r}', \mathbf{r}\right). \tag{14}$$

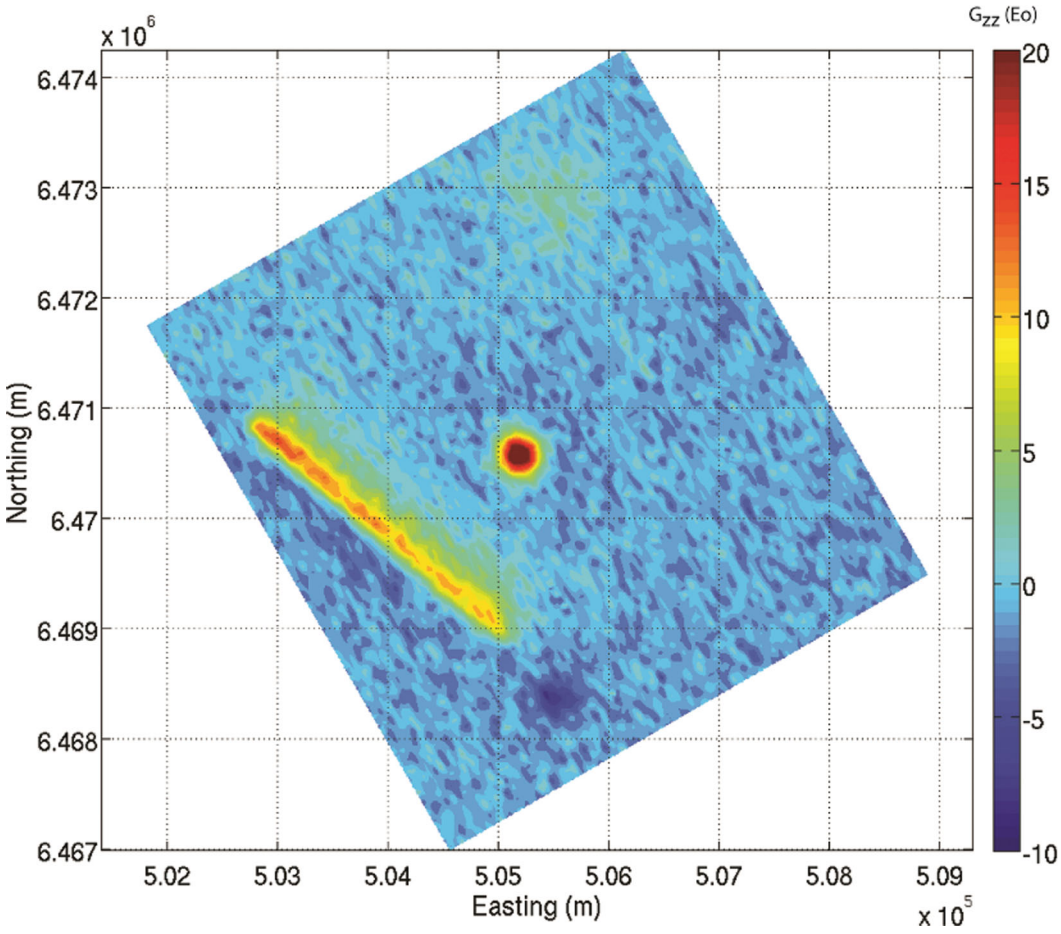

Figure 7. 2.67 g cm^{-3} terrain corrected G_{zz} data calculated using the 3-D Cauchy-type integral method.

This last equation can be written in matrix form using matrix notations for the Cauchy integral (7):

$$g_\alpha\left(\mathbf{r}'\right) = -\frac{1}{3}G\rho_0 \iint_S \Delta_{\alpha\beta\gamma\eta} r_\beta \frac{r_\eta - r'_\eta}{|\mathbf{r}-\mathbf{r}'|^3} n_\gamma ds,$$

$$\alpha, \beta, \gamma, \eta = x, y, z. \tag{15}$$

Note that, the right hand sides of eq. (13) can be unified, taking into account that the function $\frac{4\pi}{3}G\rho_0\mathbf{r}'$ is constant under $\mathbf{r}$ and, according to eq. (3):

$$\mathbf{C}^S\left(\mathbf{r}', \mathbf{r}'\right) = \begin{cases} \mathbf{r}', & \mathbf{r}' \in D, \\ 0, & \mathbf{r}' \in CD. \end{cases} \tag{16}$$

Therefore, we arrive at the following unified expression for gravity field, which holds both inside and outside of masses:

$$\mathbf{g}\left(\mathbf{r}'\right) = \frac{4\pi}{3}G\rho_0\left[\mathbf{C}^S\left(\mathbf{r}', \mathbf{r}\right) - \mathbf{C}^S\left(\mathbf{r}', \mathbf{r}'\right)\right]$$

$$= \frac{4\pi}{3}G\rho_0\mathbf{C}^S\left(\mathbf{r}', \left(\mathbf{r}-\mathbf{r}'\right)\right). \tag{17}$$

This last equation can also be represented in matrix notation as follows:

$$g_\alpha\left(\mathbf{r}'\right) = -\frac{1}{3}G\rho_0 \iint_S \Delta_{\alpha\beta\gamma\eta} \frac{\left(r_\beta - r'_\beta\right)\left(r_\eta - r'_\eta\right)}{|\mathbf{r}-\mathbf{r}'|^3} n_\gamma ds,$$

$$\alpha, \beta, \gamma, \eta = x, y, z. \tag{18}$$

We should note that, when the density ρ_0 is constant there is a simple formula that could be derived from the Newton's integral directly using the second vector statement of the Gauss theorem (Zhdanov 1988), namely

$$\mathbf{g}\left(\mathbf{r}'\right) = -G\rho_0 \iint_S \frac{\mathbf{n}}{|\mathbf{r}-\mathbf{r}'|} ds. \tag{19}$$

However, the surface integral in eq. (19) does not have the analytical properties of the Cauchy-type integral, and when ρ is variable, this approach should imply differentiating ρ, which may result in rather complicated and unstable numerical procedures. We will demonstrate below that the properties of the Cauchy-type integrals make it possible to derive very elegant and numerically efficient expressions for the gravity field and its gradients, which makes this technique attractive for applications.

3.2 Representing the gravity gradients in terms of 3-D Cauchy-type integrals

The gravity gradients can be represented as a tensor, $\widehat{\mathbf{g}}(\mathbf{r}')$, whose scalar components can be expressed as the first spatial derivatives of the gravity field

$$g_{\alpha\nu} = \frac{\partial g_\alpha}{\partial r_\nu}, \ \alpha, \nu = x, y, z. \tag{20}$$

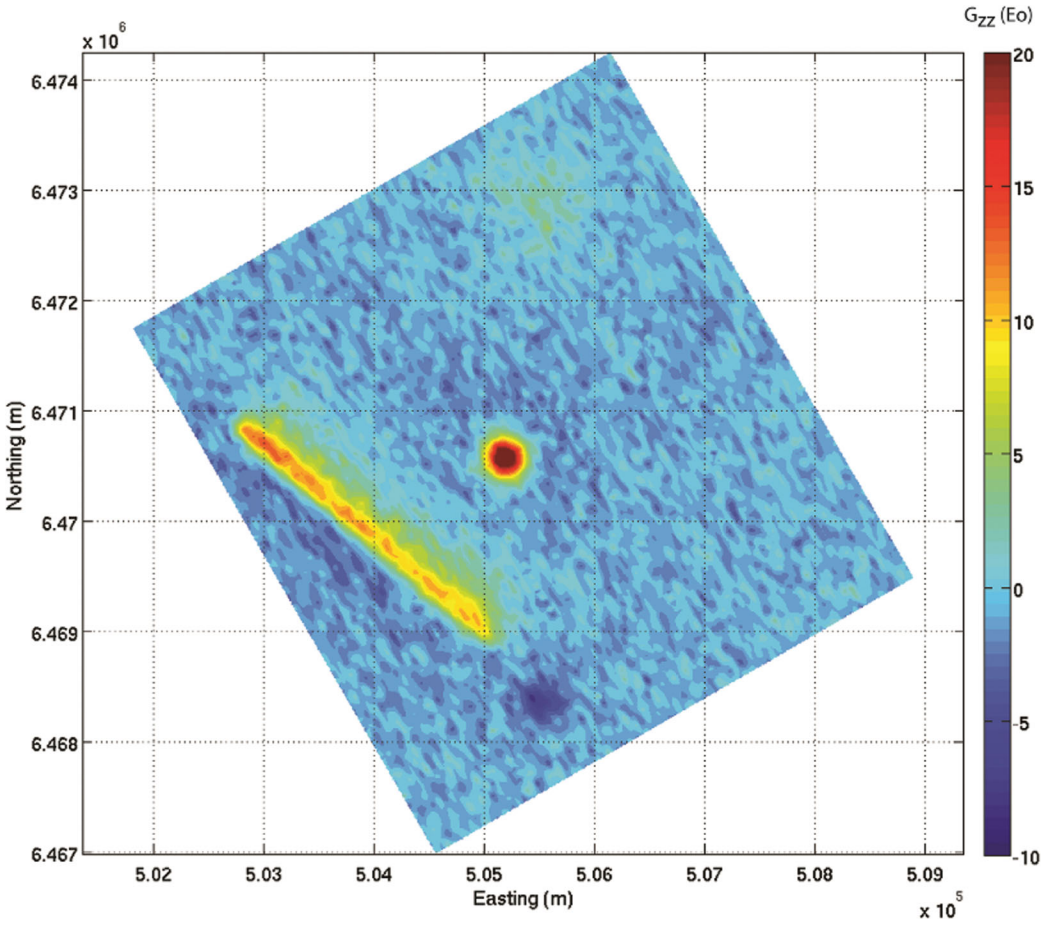

Figure 8. 2.67 g cm^{-3} terrain corrected G_{zz} data calculated using prisms (Courtesy of RTX).

Substituting eq. (15) into eq. (20), we have

$$g_{\alpha\nu}\left(\mathbf{r}'\right) = \frac{\partial g_\alpha\left(\mathbf{r}'\right)}{\partial \nu'}$$

$$= -\frac{1}{3}G\rho_0 \iint_S \Delta_{\alpha\beta\gamma\eta} r_\beta \frac{\partial}{\partial r'_\nu}\left(\frac{r_\eta - r'_\eta}{\left|\mathbf{r}-\mathbf{r}'\right|^3}\right) ds;$$

$$\alpha, \beta, \gamma, \eta = x, y, z. \tag{21}$$

Taking into account:

$$\frac{\partial}{\partial r'_\nu}\left(\frac{r_\eta - r'_\eta}{\left|\mathbf{r}-\mathbf{r}'\right|^3}\right) = \frac{1}{\left|\mathbf{r}-\mathbf{r}'\right|^5}\left[3\left(r_\nu - r'_\nu\right)\left(r_\eta - r'_\eta\right) - \left|\mathbf{r}-\mathbf{r}'\right|^2 \delta_{\nu\eta}\right],$$

we have the following matrix notation for the gravity gradients which holds both inside and outside of masses:

$$g_{\alpha\nu}\left(\mathbf{r}'\right) = -G\rho_0 \iint_S \Delta_{\alpha\beta\gamma\eta} \frac{r_\beta}{\left|\mathbf{r}-\mathbf{r}'\right|^5}$$

$$\times \left[3\left(r_\nu - r'_\nu\right)\left(r_\eta - r'_\eta\right) - \left|\mathbf{r}-\mathbf{r}'\right|^2 \delta_{\nu\eta}\right] n_\gamma ds. \tag{22}$$

In the above equation, we have assumed that the density inside the domain D is constant. However, as discussed by Zhdanov (1988), the density of the domain can be any arbitrary continuous function, $\rho(\mathbf{r})$. This means we are able to modify the above (and following) equations to incorporate any of the analytic density-depth functions in use for describing sedimentary basins, such as linear, quadratic, parabolic, exponential, hyperbolic and polynomial functions. Some examples of the variable density function are considered below in Section 4.4.

3.3 Cauchy-type representation of the gravity field and its gradients for terrain with uniform density

Let us consider a 3-D density model with a density contrast at some surface Γ, that represents the terrain. We will refer to Γ as the *density contrast surface*. We can consider the 3-D density model to be infinitely extended in the horizontal directions with domain D bounded by the surface Γ, described by equation $z = h(x, y) - H_0$, and a horizontal plane P , $z = -H_0$ (Fig. 1), where $H_0 \geq h(x, y) \geq 0$ and:

$$h\left(x, y\right) - H_1 \to 0 \text{ for } \sqrt{x^2 + y^2} \to \infty,$$

where H_1 is a constant. For terrain correction of gravity data, the surface Γ represents the terrain, and the horizontal plane P intersects mean sea level (e.g. Kirby & Featherstone 2002). In the standard practice of terrain correction for gravity gradiometry data, the surface Γ represents the terrain, and the horizontal plane P intersects the lowest point in the terrain.

It was shown by Zhdanov (1988) that the gravity field, $\mathbf{g}$, of the infinitely extended domain can be represented as the following Cauchy-type integral

$$\mathbf{g}\left(\mathbf{r}'\right) = 4\pi G\rho_0 \mathbf{C}^\Gamma\left(\mathbf{r}', \left(z + H_0\right)\mathbf{d}_z\right). \tag{23}$$

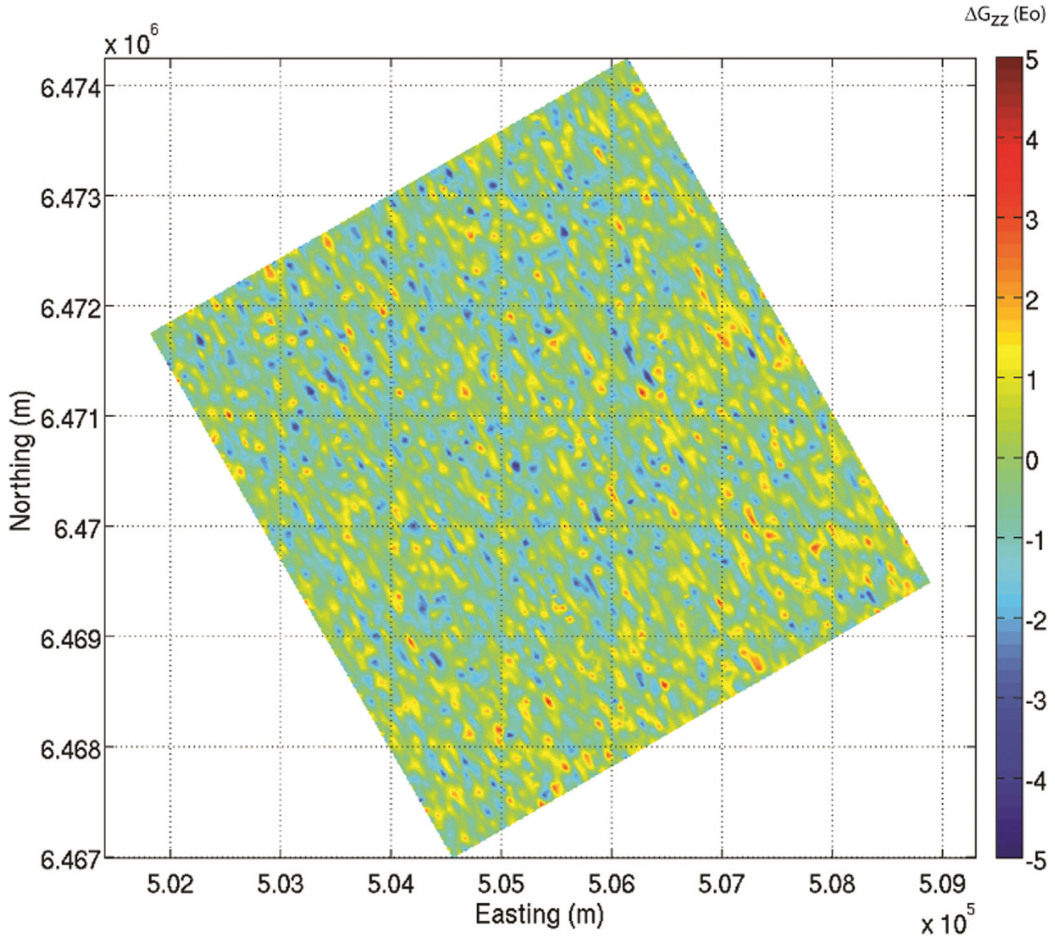

Figure 9. Difference between the 2.67 g cm^{-3} terrain corrected G_{zz} data calculated using the 3-D Cauchy-type integral method and the synthetic, noise free G_{zz} data calculated by RTX using *ModelVision*. The average difference is 0.34 Eö.

This last equation can be rewritten using matrix notations for the Cauchy integral (7):

$$g_\alpha(\mathbf{r}') = -G\rho_0 \iint_S \Delta_{\alpha z\gamma\eta}(z+H_0)\frac{r_\eta - r'_\eta}{|\mathbf{r}-\mathbf{r}'|^3} n_\gamma ds,$$

$$\alpha,\gamma,\eta = x,y,z. \tag{24}$$

In a similar way, using matrix notation, the gravity gradients can be expressed as

$$g_{\alpha\nu}(\mathbf{r}') = \frac{\partial g_\alpha(\mathbf{r}')}{\partial r'_\nu} = -G\rho_0 \iint_S \Delta_{\alpha z\gamma\eta}\frac{(z+H_0)}{|\mathbf{r}-\mathbf{r}'|^5} \times \left[3\left(r_\nu - r'_\nu\right)\left(r_\eta - r'_\eta\right) - |\mathbf{r}-\mathbf{r}'|^2 \delta_{\nu\eta}\right] n_\gamma ds. \tag{25}$$

We can provide the explicit expression for the components of the gravity field and its gradients of the density contact surface, taking into account the following relations for the components of the unit normal vector to the surface Γ

$$n_x ds = -\frac{\partial h(x,y)}{\partial x}dxdy = b_x(x,y)\,dxdy,$$

$$n_y ds = -\frac{\partial h(x,y)}{\partial y}dxdy = b_y(x,y)\,dxdy,$$

$$n_z ds = b_z(x,y)\,dxdy, \quad (z+H_0) = \Delta z(x,y), \tag{26}$$

where

$$b_x(x,y) = -\frac{\partial h(x,y)}{\partial x}, \quad b_y(x,y) = -\frac{\partial h(x,y)}{\partial y}, \quad b_z(x,y) = 1.$$

Substituting eq. (26) into eqs (24) and (25), we have

$$g_\alpha(\mathbf{r}') = -\gamma\rho_0 \int_{-\infty}^{\infty}\int \Delta_{\alpha z\gamma\eta} h(x,y)\frac{\widetilde{r}_\eta - r'_\eta}{|\widetilde{\mathbf{r}}-\mathbf{r}'|^3} b_\gamma(x,y)\,dxdy,$$

$$\alpha,\gamma,\eta = x,y,z, \tag{27}$$

and

$$g_{\alpha\nu}(\mathbf{r}') = -\gamma\rho_0 \int_{-\infty}^{\infty}\int \Delta_{\alpha z\gamma\eta}\frac{h(x,y)}{|\widetilde{\mathbf{r}}-\mathbf{r}'|^5}\left[3\left(\widetilde{r}_\nu - r'_\nu\right)\left(\widetilde{r}_\eta - r'_\eta\right) - |\widetilde{\mathbf{r}}-\mathbf{r}'|^2\delta_{\nu\eta}\right] b_\gamma(x,y)\,dxdy, \tag{28}$$

where:

$$|\widetilde{\mathbf{r}}-\mathbf{r}'| = \sqrt{(x-x')^2 + (y-y')^2 + (h(x,y) - H_0 - z')^2},$$

$$\widetilde{r}_\nu = x, \quad \widetilde{r}_y = y, \quad \widetilde{r}_z = h(x,y) - H_0, \tag{29}$$

We have arrived at the Cauchy-type integrals (27) and (28) in an analytic form. In practice, these equations need to be discretized and solved numerically. This will be discussed in a subsequent section of this paper.

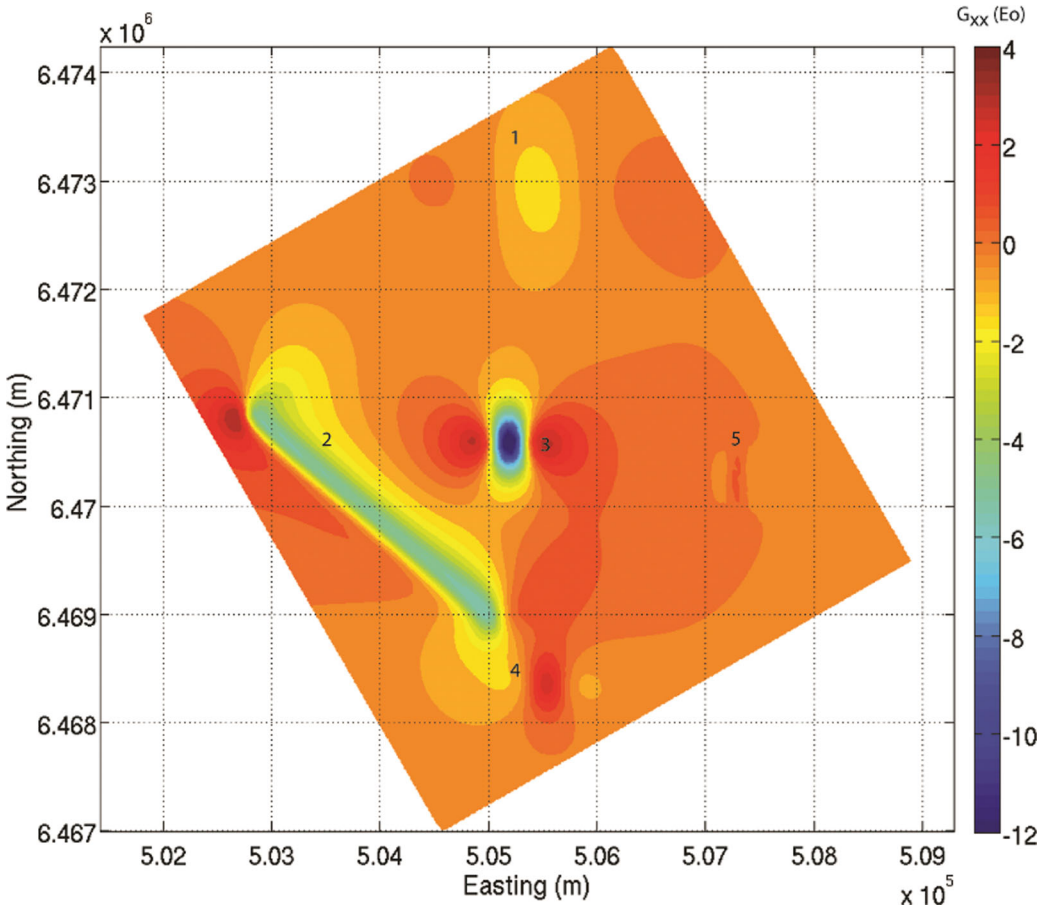

Figure 10. Synthetic, noise-free G_{xx} data calculated by RTX using *ModelVision* with no terrain effect. Each of the targets are identified by their corresponding number in Table 1.

3.4 Cauchy-type representation of the gravity field and its gradients for terrain with variable density

For sedimentary basins, terrain (or bathymetry) corrections are generally calculated as the response due to the volume of earth bound by an upper surface of the digital elevation (bathymetry) model and a lower surface of a plane at depth (G. Jorgensen, personal communication, 2011). To simulate sediment compaction and diagenesis causing a loss of porosity, densities are often parameterized using empirically derived analytic density-depth functions with the terrain (or bathymetry) forming the datum. As discussed by Zhou (2008, 2009), the variety of analytic density-depth functions in use span linear, quadratic, parabolic, exponential, hyperbolic and polynomial functions. Generally, we can express this variable density as:

$$\rho = \rho(z).$$

In this case, it can be shown that the gravity field, $\mathbf{g}$, of an infinitely extended domain can be represented as the following Cauchy-type integral

$$\mathbf{g}\left(\mathbf{r}'\right) = 4\pi G\rho_0 \mathbf{C}^{\Gamma}\left(\mathbf{r}', \left[R\left(z\right) - R\left(-H_0\right)\right]\mathbf{d}_z\right), \tag{30}$$

where $R(z)$ is any indefinite integral of the density

$$R(z) = \int \rho(z)\mathrm{d}z. \tag{31}$$

For example, for a terrain with a linear vertical variation in density: $\rho(z) = \rho_0 + az$, then

$$R(z) = \rho_0 z + \frac{1}{2}az^2.$$

As another example, for a body with an exponential vertical variation in density: $\rho(z) = \rho_0 + a\exp(kz)$, then

$$R(z) = \rho_0 z + \frac{a}{k}\exp(kz).$$

Eq. (30) can be rewritten using matrix notations for the Cauchy integral (7)

$$g_\alpha\left(\mathbf{r}'\right) = -G\iint_S \Delta_{\alpha z\gamma\eta}\left[R\left(z\right) - R\left(-H_0\right)\right]\frac{r_\eta - r'_\eta}{\left|\mathbf{r}-\mathbf{r}'\right|^3}n_\gamma ds,$$
$$\alpha, \gamma, \eta = x, y, z. \tag{32}$$

In a similar way, using matrix notation, the gravity gradients can be expressed as:

$$g_{\alpha\nu}\left(\mathbf{r}'\right) = \frac{\partial g_\alpha\left(\mathbf{r}'\right)}{\partial r'_\nu} = -G\iint_S \Delta_{\alpha z\gamma\eta}\frac{R\left(z\right) - R\left(-H_0\right)}{\left|\mathbf{r}-\mathbf{r}'\right|^5} \times\left[3\left(r_\nu - r'_\nu\right)\left(r_\eta - r'_\eta\right) - \left|\mathbf{r}-\mathbf{r}'\right|^2\delta_{\nu\eta}\right]n_\gamma ds. \tag{33}$$

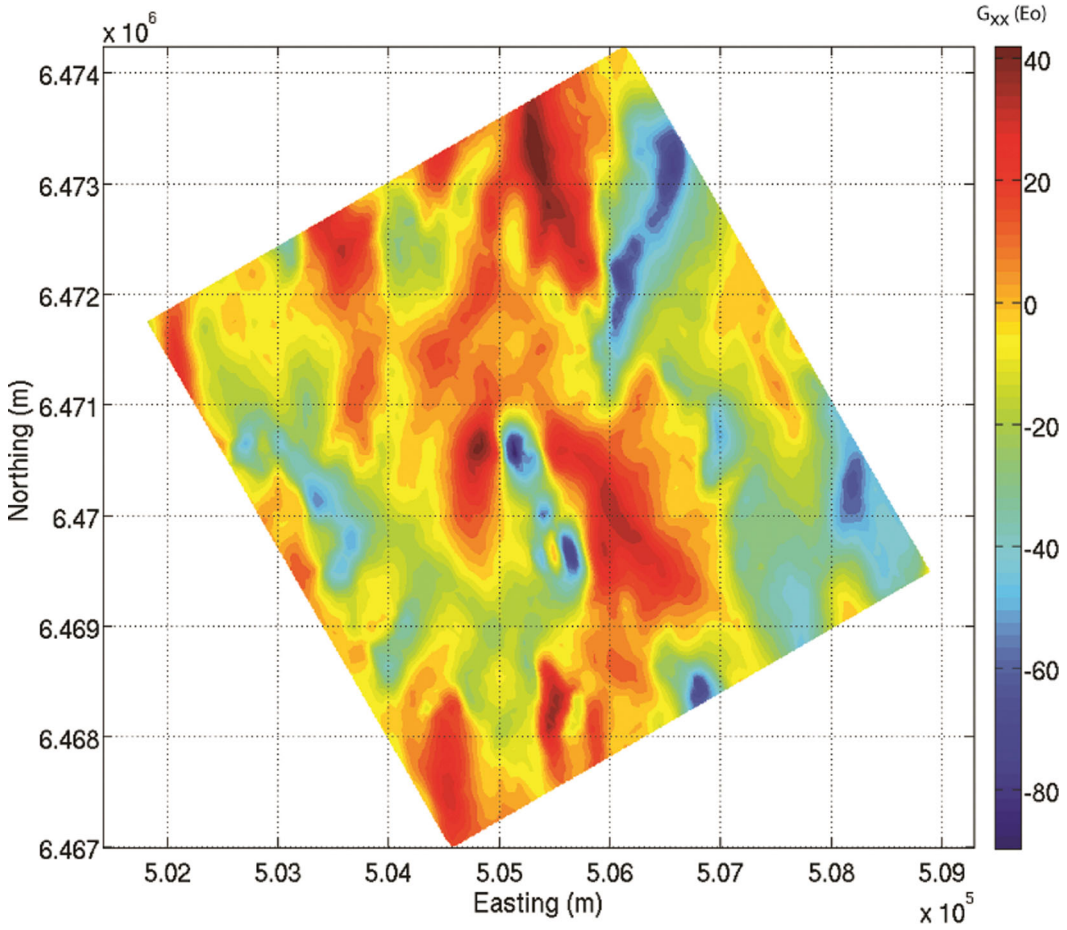

Figure 11. Synthetic free-air G_{xx} data calculated by RTX with terrain effect added, contaminated with noise representative of a 1 Eö/$\sqrt{\text{Hz}}$ (at 1 Hz) instrument.

We can provide the explicit expressions for the gravity field and its gradients of the density contact surface, taking into account relations (26) for the components of the unit normal vector to the surface, Γ

$$g_\alpha\left(\mathbf{r}'\right) = -G\int\limits_{-\infty}^{\infty}\int \Delta_{\alpha z\gamma\eta}\left[R\left(z\right) - R\left(-H_0\right)\right]$$

$$\times \frac{\widetilde{r}_\eta - r'_\eta}{\left|\widetilde{\mathbf{r}} - \mathbf{r}'\right|^3} b_\gamma\left(x, y\right) dxdy, \alpha, \gamma, \eta = x, y, z, \qquad (34)$$

and:

$$g_{\alpha\nu}\left(\mathbf{r}'\right) = -G\int\limits_{-\infty}^{\infty}\int \Delta_{\alpha z\gamma\eta}\frac{R\left(z\right) - R\left(-H_0\right)}{\left|\widetilde{\mathbf{r}} - \mathbf{r}'\right|^5}\left[3\left(\widetilde{r}_\nu - r'_\nu\right)\right.$$

$$\left.\times\left(\widetilde{r}_\eta - r'_\eta\right) - \left|\widetilde{\mathbf{r}} - \mathbf{r}'\right|^2\delta_{\nu\eta}\right] b_\gamma(x, y)dxdy. \qquad (35)$$

We also note that as discussed by Zhdanov (1988), the density function may also vary with horizontal position as well as depth, that is, $\rho(x, y, z)$.

4 DISCRETE FORMS OF THE CAUCHY-TYPE REPRESENTATION OF THE GRAVITY FIELD AND ITS GRADIENTS

4.1 Rectangular discretization of the density contrast surface

We can discretize the Cauchy-type integrals (27) and (28) for the gravity field and its gradients by dividing the horizontal integration plane XY into a rectangular grid of N_m cells with constant discretization of Δx and Δy in the x and y directions, respectively. This is appropriate for DEMs, as they are usually gridded to a constant spatial discretization. We assume that within each cell, P_k ($k = 1, 2, \ldots N_m$), the corresponding part of the density contact surface can be represented by an element of a plane described by the equation

$$z = h\left(x, y\right) - H_0 = h^{(k)} - b_x^{(k)}\left(x - x_k\right) - b_y^{(k)}\left(y - y_k\right)$$

$$-H_0, \left(x, y\right) \in P_k, \qquad (36)$$

where (x_k, y_k) denotes the centre of the cell P_k. In this case, we have:

$$b_x\left(x, y\right) = b_x^{(k)}, \quad b_y\left(x, y\right) = b_y^{(k)}, \quad b_z\left(x, y\right) = b_z^{(k)} = 1,$$

$$\left(x, y\right) \in P_k,$$

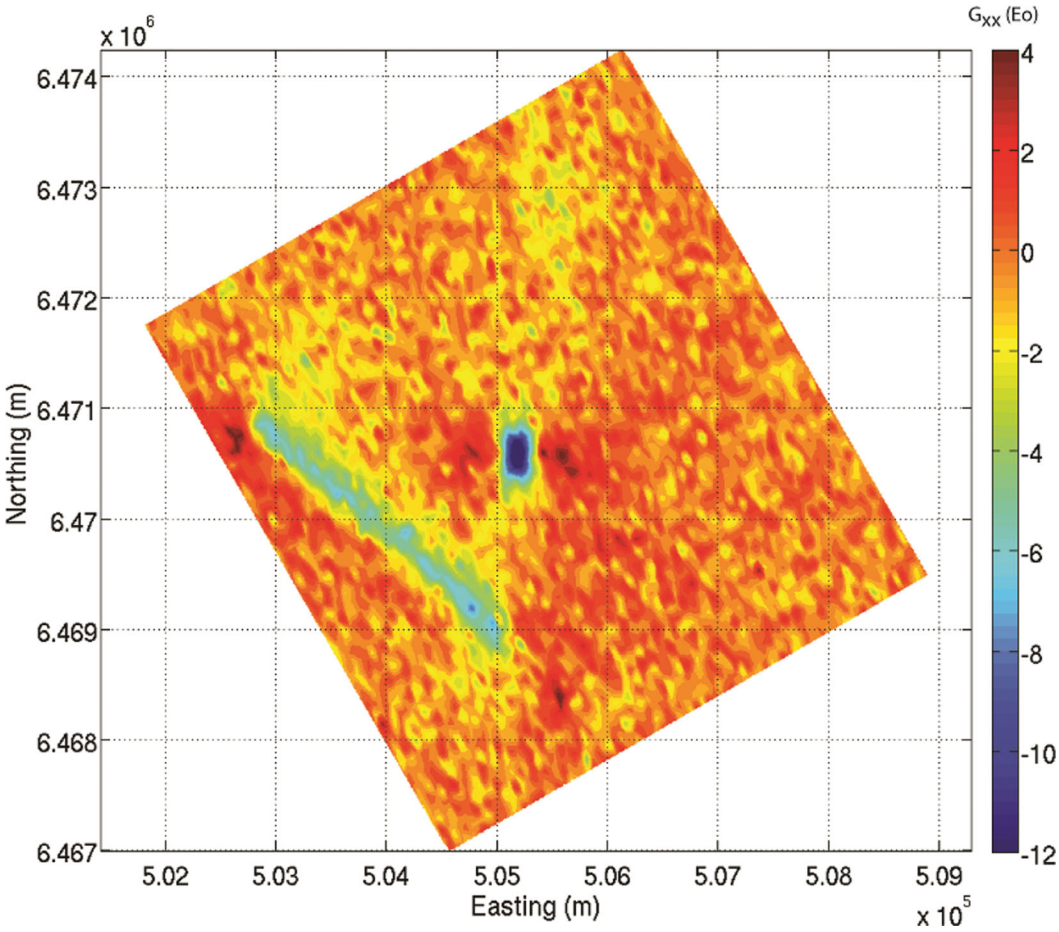

Figure 12. 2.67 g cm^{-3} terrain corrected G_{xx} data calculated using the 3-D Cauchy-type integral method.

and eq. (27) for gravity field takes the form

$$g_\alpha\left(\mathbf{r}'\right) = -G\rho_0 \sum_{k=1}^{N_m} \iint_{P_k} \Delta_{\alpha z\gamma\eta} h\left(x,y\right) \frac{\widetilde{r}_\eta - r'_\eta}{\left|\widetilde{\mathbf{r}} - \mathbf{r}'\right|^3} b_\gamma^{(k)} dxdy,$$
$$\alpha,\gamma,\eta = x,y,z. \tag{37}$$

Using the discrete model parameters introduced above, and discrete gravity data, $g_\alpha(\mathbf{r}'_n)$, we can represent the forward modelling operator for the gravity field (37) of the density contact surface Γ as:

$$g_\alpha\left(\mathbf{r}'_n\right) = \sum_{k=1}^{N_m} f_{\alpha\gamma}^{(nk)} h^{(k)} b_\gamma^{(k)}, \tag{38}$$

where:

$$f_{\alpha\gamma}^{(nk)} = -G\rho_0 \Delta_{\alpha z\gamma\eta} \frac{\widetilde{r}_\eta^{(k)} - r_\eta^{(n)\prime}}{\left|\widetilde{\mathbf{r}}_k - \mathbf{r}'_n\right|^3} \Delta x \Delta y, \tag{39}$$

and:

$$\left|\widetilde{\mathbf{r}}_k - \mathbf{r}'_n\right| = \sqrt{\left(x_k - x'_n\right)^2 + \left(y_k - y'_n\right)^2 + \left(h^{(k)} - H_0 - z'_n\right)^2},$$
$$\widetilde{r}_x^{(k)} = x_k, \quad \widetilde{r}_y^{(k)} = y_k, \quad \widetilde{r}_z^{(k)} = h^{(k)} - H_0; \quad \widetilde{r}_x^{(n)\prime} = x'_n, \quad \widetilde{r}_y^{(n)\prime} = y'_n,$$
$$\widetilde{r}_z^{(n)\prime} = z'_n. \tag{40}$$

In a similar way, the discrete form of expression (28) for gravity gradients can be written as:

$$g_{\alpha\nu}\left(\mathbf{r}'\right) = -G\rho_0 \sum_{k=1}^{N_m} \iint_{P_k} \Delta_{\alpha z\gamma\eta} \frac{h\left(x,y\right)}{\left|\widetilde{\mathbf{r}} - \mathbf{r}'\right|^5}$$
$$\times \left[3\left(\widetilde{r}_\nu - r'_\nu\right)\left(\widetilde{r}_\eta - r'_\eta\right) - \left|\widetilde{\mathbf{r}} - \mathbf{r}'\right|^2 \delta_{\nu\eta}\right] b_\gamma^{(k)} dxdy. \tag{41}$$

Using the discrete model parameters introduced above, and discrete gravity gradient data, $g_{\alpha\nu}(\mathbf{r}'_n)$, we can represent the forward modelling operator for the gravity gradients (41) of the density contact surface Γ as

$$g_{\alpha\nu}\left(\mathbf{r}'_n\right) = \sum_{k=1}^{N_m} F_{\alpha\nu\gamma}^{(nk)} h^{(k)} b_\gamma^{(k)}, \tag{42}$$

where:

$$F_{\alpha\nu\gamma}^{(nk)} = -G\rho_0 \Delta_{\alpha z\gamma\eta} \frac{1}{\left|\widetilde{\mathbf{r}}_k - \mathbf{r}'_n\right|^5}$$
$$\times \left[3\left(\widetilde{r}_\nu^{(k)} - r_\nu^{(n)\prime}\right)\left(\widetilde{r}_\eta^{(k)} - r_\eta^{(n)\prime}\right) - \left|\widetilde{\mathbf{r}}_k - \mathbf{r}'_n\right|^2 \delta_{\nu\eta}\right] \Delta x \Delta y. \tag{43}$$

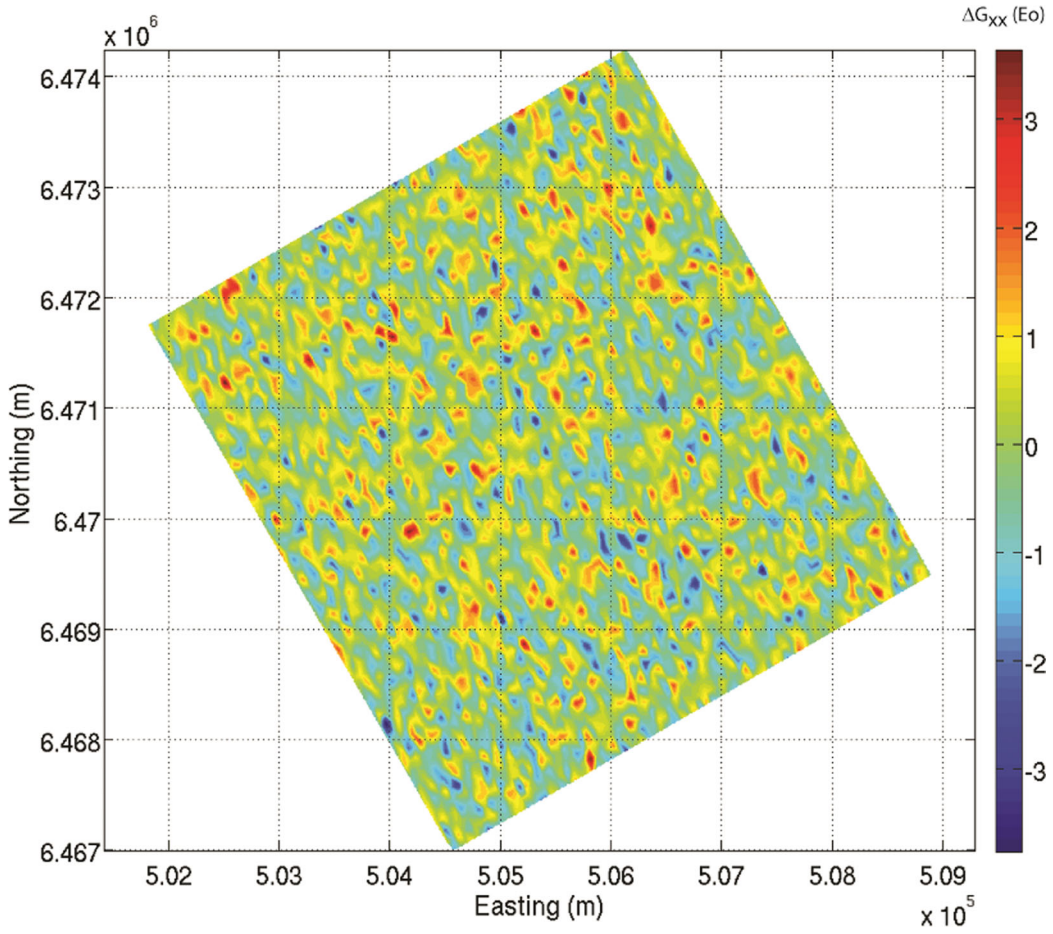

Figure 13. Difference between the 2.67 g cm^{-3} terrain corrected G_{xx} data calculated using the 3-D Cauchy-type integral method and the synthetic, noise free G_{xx} data calculated by RTX using *ModelVision*. The average difference is 0.35 Eö.

4.2 Triangular discretization of the density contrast surface

We assume, as above, that the function $h(x, y)$, describing the density contrast surface Γ,is given on a rectangular mesh $\sum$

$$\sum = \left\{ (x_i, y_j) \quad \begin{array}{lll} x_1 = x', & x_I = x'', & x_{i+1} = x_i + \Delta x, \\ & & i = 1, 2, \ldots, I, \\ y_1 = y', & y_J = y'', & y_{j+1} = y_j + \Delta y, \\ & & j = 1, 2, \ldots, J. \end{array} \right\}$$

In this case, the coordinates of the points located on the surface Γ,$\widetilde{\mathbf{r}}_k = \widetilde{\mathbf{r}}_{ij} \in \Gamma$, are as follows:

$$\widetilde{\mathbf{r}}_k = \left(x_k, y_k, h^{(k)} - H_0\right) = \left(x_i, y_j, h^{(ij)} - H_0\right) = \widetilde{\mathbf{r}}_{ij},$$

where $h^{(k)} = h^{(ij)} = h\left(x_i, x_j\right)$. (44)

Note that, the nodes of the mesh are numbered consecutively along the East and North directions. For the given numbering of the nodes, $k = 1, 2, 3, \ldots, K, (K = IJ)$, one can establish a simple one-to-one relationship between the index n and the double number (i, j)

$$k = i + (j - 1)K. \tag{45}$$

We can divide each rectangular cell of the mesh $\sum$ into two triangles which would form the elementary cells P_{Lk} (left triangular) and P_{Lk} (right triangular), as shown in Fig. 2. The corresponding equations of the plane parts, Γ_{Lk} and Γ_{Rk}, of the surface Γ, located just above the cells P_{Lk} and P_{Rk} can be written using the equations of the plane through the corresponding points $\widetilde{\mathbf{r}}_{ij}, \widetilde{\mathbf{r}}_{i+1,j}, \widetilde{\mathbf{r}}_{i+1,j+1}$ and $\widetilde{\mathbf{r}}_{ij}, \widetilde{\mathbf{r}}_{i,j+1}, \widetilde{\mathbf{r}}_{i+1,j+1}$, for the left and right triangulars, respectively:

$$\left(\mathbf{r} - \widetilde{\mathbf{r}}_{ij}\right) \cdot \left[\left(\widetilde{\mathbf{r}}_{i+1,j} - \widetilde{\mathbf{r}}_{ij}\right) \times \left(\widetilde{\mathbf{r}}_{i+1,j+1} - \widetilde{\mathbf{r}}_{ij}\right)\right] = 0, \text{ for } \Gamma_{Lk}, \tag{46}$$

and

$$\left(\mathbf{r} - \widetilde{\mathbf{r}}_{ij}\right) \cdot \left[\left(\widetilde{\mathbf{r}}_{i,j+1} - \widetilde{\mathbf{r}}_{ij}\right) \times \left(\widetilde{\mathbf{r}}_{i+1,j+1} - \widetilde{\mathbf{r}}_{ij}\right)\right] = 0, \text{ for } \Gamma_{Rk}. \tag{47}$$

We can write an equivalent form of eq. (46):

$$a_{Lx}^{(k)} x + a_{Ly}^{(k)} y + a_{Lz}^{(k)} z + a_{L0}^{(k)} = 0, \tag{48}$$

where:

$$a_{Lx}^{(k)} = \begin{vmatrix} 1 & y_{ij} & z_{ij} \\ 1 & y_{i+1,j} & z_{i+1,j} \\ 1 & y_{i+1,j+1} & z_{i+1,j+1} \end{vmatrix},$$

$$a_{Ly}^{(k)} = \begin{vmatrix} x_{ij} & 1 & z_{ij} \\ x_{i+1,j} & 1 & z_{i+1,j} \\ x_{i+1,j+1} & 1 & z_{i+1,j+1} \end{vmatrix}, \tag{49}$$

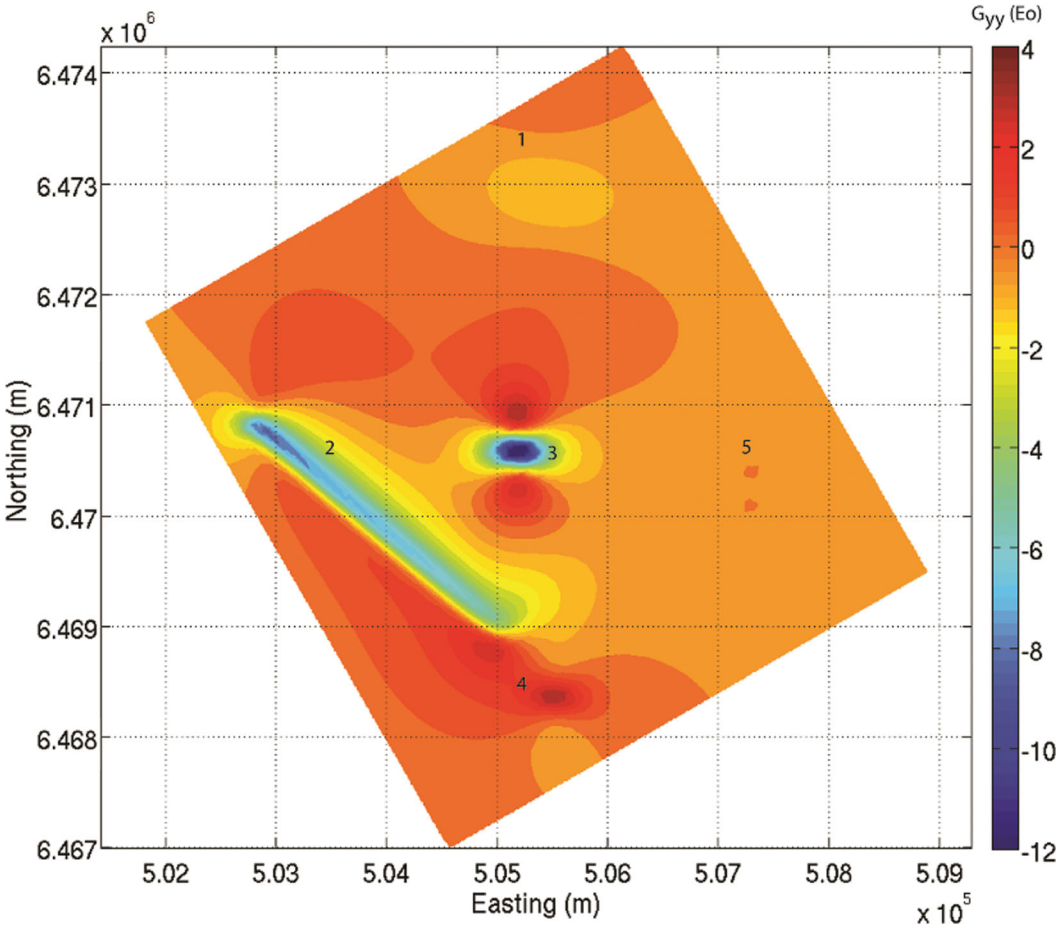

Figure 14. Synthetic, noise-free G_{yy} data calculated by RTX using *ModelVision*with no terrain effect. Each of the targets are identified by their corresponding number in Table 1.

$$a_{Lx}^{(k)} = \begin{vmatrix} x_{ij} & y_{ij} & 1 \\ x_{i+1,j} & y_{i+1,j} & 1 \\ x_{i+1,j} & y_{i+1,j+1} & 1 \end{vmatrix},$$

$$a_{L0}^{(k)} = \begin{vmatrix} x_{ij} & y_{ij} & z_{ij} \\ x_{i+1,j} & y_{i+1,j} & z_{i+1,j} \\ x_{i+1,j} & y_{i+1,j+1} & z_{i+1,j+1} \end{vmatrix}. \tag{50}$$

Similarly, we can write an equivalent form of eq. (47):

$$a_{Rx}^{(k)} x + a_{Ry}^{(k)} y + a_{Rz}^{(k)} z + a_{R0}^{(k)} = 0, \tag{51}$$

where:

$$a_{Rx}^{(k)} = \begin{vmatrix} 1 & y_{ij} & z_{ij} \\ 1 & y_{i,j+1} & z_{i,j+1} \\ 1 & y_{i+1,j+1} & z_{i+1,j+1} \end{vmatrix},$$

$$a_{Ry}^{(k)} = \begin{vmatrix} x_{ij} & 1 & z_{ij} \\ x_{i,j+1} & 1 & z_{i,j+1} \\ x_{i+1,j+1} & 1 & z_{i+1,j+1} \end{vmatrix}, \tag{52}$$

$$a_{Rx}^{(k)} = \begin{vmatrix} x_{ij} & y_{ij} & 1 \\ x_{i,j+1} & y_{i,j+1} & 1 \\ x_{i+1,j} & y_{i+1,j+1} & 1 \end{vmatrix},$$

$$a_{R0}^{(k)} = \begin{vmatrix} x_{ij} & y_{ij} & z_{ij} \\ x_{i,j+1} & y_{i,j+1} & z_{i,j+1} \\ x_{i+1,j} & y_{i+1,j+1} & z_{i+1,j+1} \end{vmatrix}. \tag{53}$$

Also, we introduce the following notations

$$h_L^{(k)} = -\left[a_{Lx}^{(k)} x_{Lk} + a_{Ly}^{(k)} y_{Lk} + a_{L0}^{(k)}\right] / a_{Lz}^{(k)}, \tag{54}$$

$$h_R^{(k)} = -\left[a_{Rx}^{(k)} x_{Rk} + a_{Ry}^{(k)} y_{Rk} + a_{R0}^{(k)}\right] / a_{Rz}^{(k)}, \tag{55}$$

where we denote (x_{Lk}, y_{Lk}) and (x_{Rk}, y_{Rk}) as the centres of the cells P_{Lk} and P_{Rk}, respectively.

Substituting eqs (54) and (55) into eq. (26), we find

$$b_{Lx}^{(k)} = a_{Lx}^{(k)} / a_{Lz}^{(k)},\ b_{Ly}^{(k)} = a_{Ly}^{(k)} / a_{Lz}^{(k)},$$
$$b_{Rx}^{(k)} = a_{Rx}^{(k)} / a_{Rz}^{(k)},\ b_{Ry}^{(k)} = a_{Ry}^{(k)} / a_{Rz}^{(k)}. \tag{56}$$

Using the discrete model parameters introduced earlier, and discrete gravity data, $g_\alpha(\mathbf{r}'_n)$, we can represent the forward modelling operator for the gravity field (37) of the density contrast surface Γ

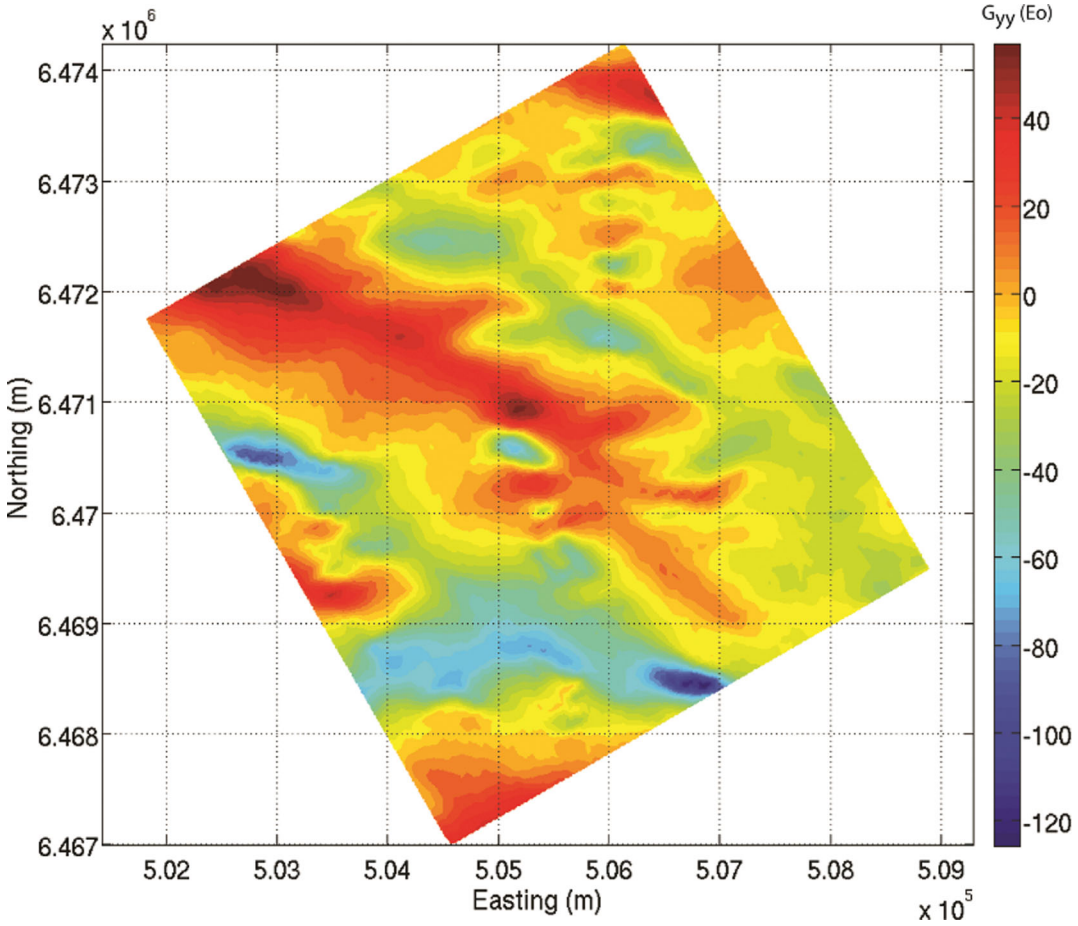

Figure 15. Synthetic free-air G_{yy} data calculated by RTX with terrain effect added, contaminated with noise representative of a 1 Eö/$\sqrt{\text{Hz}}$ (at 1 Hz) instrument.

as

$$g_\alpha(\mathbf{r}') = \sum_{k=1}^{K} f_{L\alpha\gamma}^{(nk)} h_L^{(k)} b_{L\gamma}^{(k)} + \sum_{k=1}^{K} f_{R\alpha\gamma}^{(nk)} h_R^{(k)} b_{R\gamma}^{(k)};\ \alpha,\gamma,\eta = x,y,z, \tag{57}$$

where:

$$f_{L\alpha\gamma}^{(nk)} = -G\rho_0 \Delta_{\alpha z\gamma\eta} \frac{\widetilde{r}_{L\eta}^{(k)} - r_\eta^{(n)\prime}}{\left|\widetilde{\mathbf{r}}_{Lk} - \mathbf{r}_n'\right|^3} \Delta x \Delta y;$$

$$f_{R\alpha\gamma}^{(nk)} = -G\rho_0 \Delta_{\alpha z\gamma\eta} \frac{\widetilde{r}_{R\eta}^{(k)} - r_\eta^{(n)\prime}}{\left|\widetilde{\mathbf{r}}_{Rk} - \mathbf{r}_n'\right|^3} \Delta x \Delta y. \tag{58}$$

and:

$$\widetilde{r}_{Lx}^{(k)} = x_{Lk}, \quad \widetilde{r}_{Ly}^{(k)} = y_{Lk}, \quad \widetilde{r}_{Lz}^{(k)} = h_L^{(k)} - H_0,$$

$$\widetilde{r}_{Rx}^{(k)} = x_{Rk}, \quad \widetilde{r}_{Ry}^{(k)} = y_{Rk}, \quad \widetilde{r}_{Rz}^{(k)} = h_R^{(k)} - H_0; \quad \widetilde{r}_x^{(n)\prime} = x_n',$$

$$\widetilde{r}_y^{(n)\prime} = y_n', \quad \widetilde{r}_z^{(n)\prime} = z_n'.$$

In a similar way, using the discrete model parameters, the discrete form of gravity gradients can be written as

$$g_{\alpha\nu}(\mathbf{r}_n') = \sum_{k=1}^{K} F_{L\alpha\gamma}^{(nk)} h_L^{(k)} b_{L\gamma}^{(k)} + \sum_{k=1}^{K} F_{R\alpha\gamma}^{(nk)} h_R^{(k)} b_{R\gamma}^{(k)};$$

$$\alpha,\gamma,\eta = x,y,z, \tag{59}$$

where

$$F_{L\alpha\gamma}^{(nk)} = -G\rho_0 \Delta_{\alpha z\gamma\eta} \frac{1}{2\left|\widetilde{\mathbf{r}}_{Lk} - \mathbf{r}_n'\right|^5} \times \left[3\left(\widetilde{r}_{Lv}^{(k)} - r_v^{(n)\prime}\right)\left(\widetilde{r}_{L\eta}^{(k)} - r_\eta^{(n)\prime}\right) - \left|\widetilde{\mathbf{r}}_{Lk} - \mathbf{r}_n'\right|^2 \delta_{v\eta}\right] \Delta x \Delta y, \tag{60}$$

$$F_{R\alpha\gamma}^{(nk)} = -G\rho_0 \Delta_{\alpha z\gamma\eta} \frac{1}{2\left|\widetilde{\mathbf{r}}_{Rk} - \mathbf{r}_n'\right|^5} \times \left[3\left(\widetilde{r}_{Rv}^{(k)} - r_v^{(n)\prime}\right)\left(\widetilde{r}_{R\eta}^{(k)} - r_\eta^{(n)\prime}\right) - \left|\widetilde{\mathbf{r}}_{Rk} - \mathbf{r}_n'\right|^2 \delta_{v\eta}\right] \Delta x \Delta y. \tag{61}$$

The significance of this method is that we can model any 3-D domain with the geometric resolution and accuracy of its DEM. Moreover, the 3-D modelling of the domain is expressed as a surface integral which may be rapidly and accurately evaluated. It is important to emphasize that, the prisms with triangulated tops (Fig. 2) provide much more accurate representation of the shape of the terrain surface than a combination of the rectangular prisms used by the conventional terrain correction methods.

Note also that, the standard practice of increasing discretization as a function of distance from the observation point can be easily incorporated into the surface integration. All together, this is particularly important for terrain correction, and represents a significant advantage of this method over volume integration methods

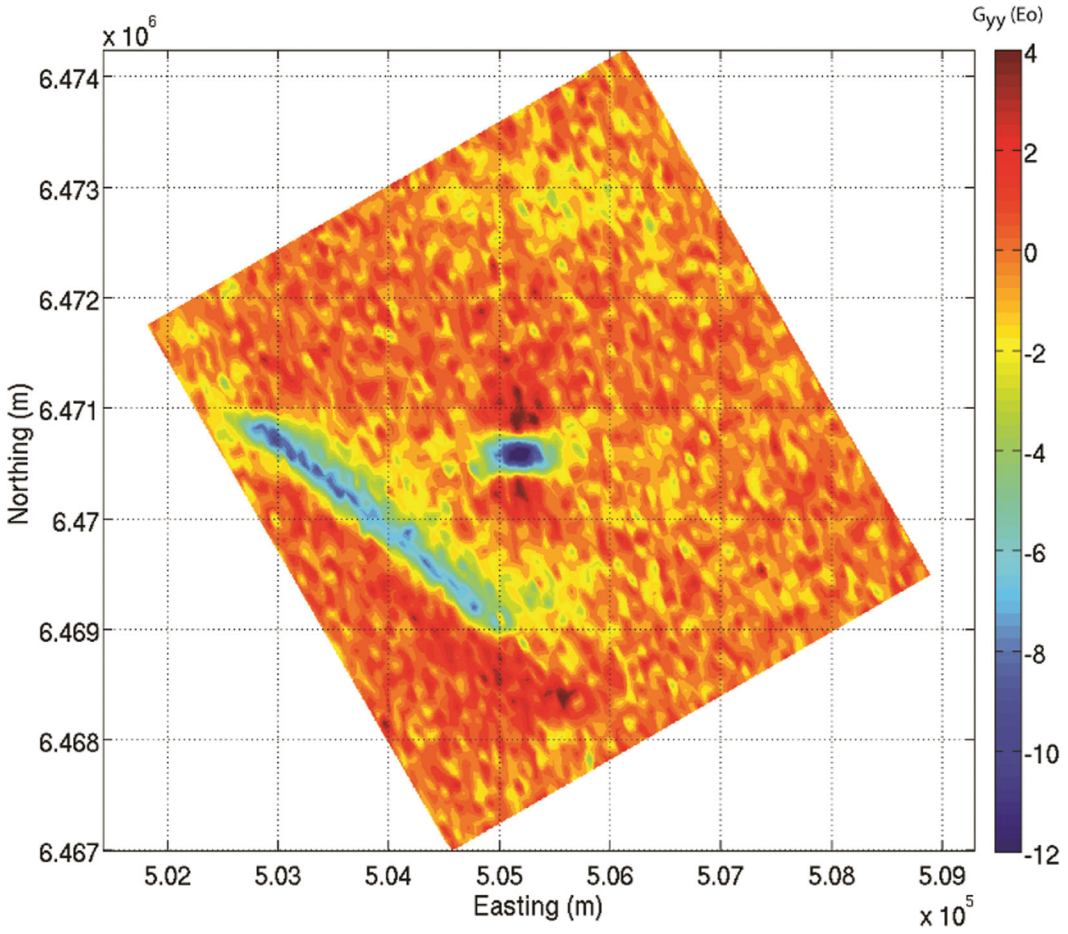

Figure 16. 2.67 g cm^{-3} terrain corrected G_{yy} data calculated using the 3-D Cauchy-type integral method.

that are fraught with issues relating to discretization and staircase approximations of the DEM.

5 MODEL STUDY: KAURING, WESTERN AUSTRALIA

With funding from the Western Australian government's 2009 Exploration Initiative Scheme and a matching contribution from Rio Tinto Exploration (RTX), the Geological Survey of Western Australia (GSWA) and Geoscience Australia (GA) have established the Kauring test site for testing and calibrating airborne gravity and gravity gradiometry systems (Howard *et al.* 2010). The site is approximately 100 km east of Perth in Western Australia, is free of low level flight restrictions, has minimal human infrastructure, and hosts gentle rolling topography of granitic terrane. The test site allows interested individuals or organizations to compare airborne data to detailed ground gravity data, or products derived from these data. It also allows for direct comparison of different airborne gravity and gravity gradiometry systems over the same gravity features where all other variables, besides the measuring system are defined and constant. DEMs have been released for 10 m LiDAR, and 80 m SRTM. Fig. 3 shows the merged LiDAR and SRTM DEMs for the area surrounding the Kauring test site. Fig. 4 shows the LiDAR DEM for the Kauring test site.

To facilitate the comparison of 3-D inversion methods during 2011, RTX developed a synthetic AGG data set of 4687 stations (Grujic 2012). The 3-D density model contained a variety of relevant geological targets representative of discrete tunnels, nickel sulfide deposits, intrusive dykes and kimberlites, embedded in a uniform 2.67 g cm^{-3} terrain so that the wavelength, magnitude and symmetry of the data were varied. The targets are summarized in Table 1. The data were simulated along a realistic drape with a mean terrain clearance of 80 m over the Kauring test site. The data for the bodies were simulated using the commercial software package, *ModelVision*.

As described by Grujic (2012, personal communications), the terrain response was simulated using concentric square zones around each observation. The cell size of the terrain information quadrupled for each consecutive zone, starting with a square of 800 m side length and 10 m cell size in the innermost zone. The size of the zones doubled for each consecutive zone. For example, the second zone around each station was a 1600 m wide square with a 40 m cell size. Six zones that follow this pattern were created around each observation. The grids were used to triangularly facet the terrain into vertical prisms with a uniform density of 2.67 g cm^{-3} that extend to a zero level datum. The response of these prisms was calculated at the measurement location. Outside the available terrain information, an infinite slab with a height equal to the mean terrain elevation was modelled and added to the responses of the prisms. The synthetic data were not filtered with any system response. Noise representative of a 1 Eö/$\sqrt{\text{Hz}}$ (at 1 Hz) instrument was then added to the simulated free-air gravity gradiometry data.

First, we consider the free-air G_{zz} data. Fig. 5 shows the noise-free G_{zz} response due to the bodies (as calculated with *ModelVision*)

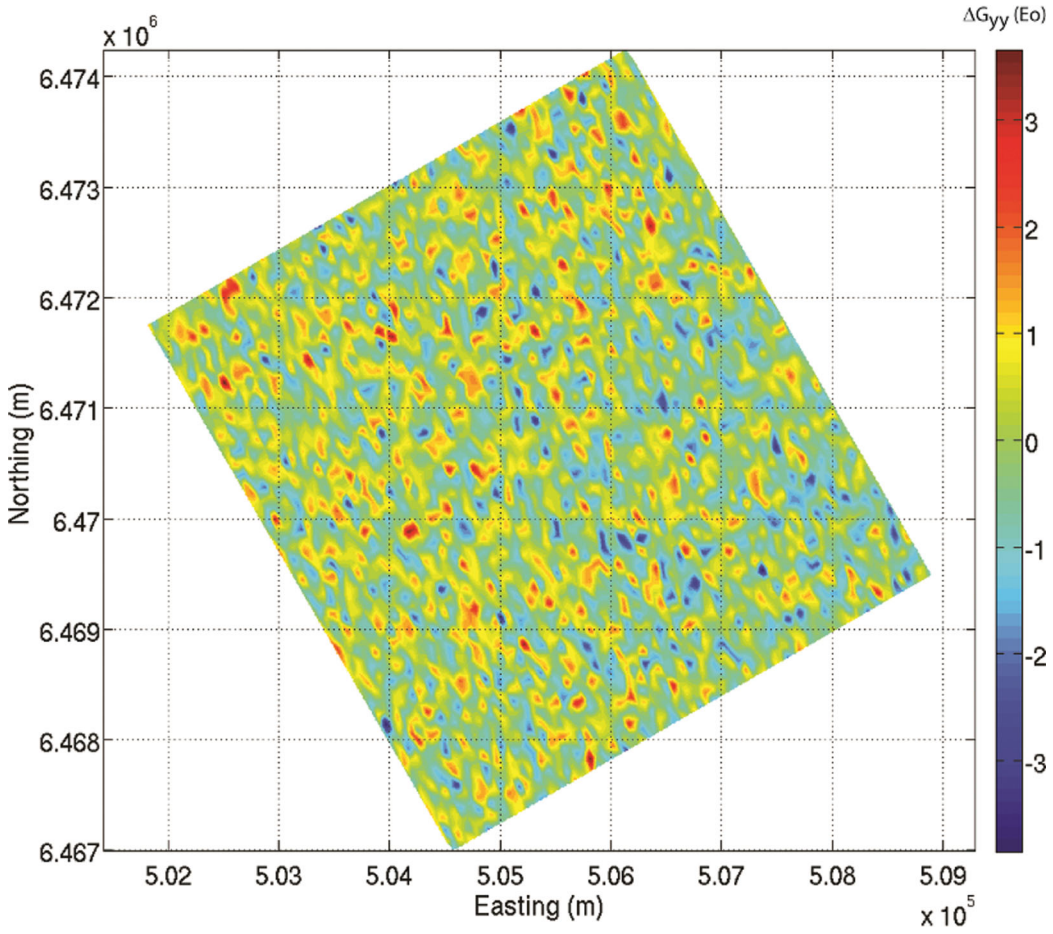

Figure 17. Difference between the 2.67 g cm^{-3} terrain corrected G_{yy} data calculated using the 3-D Cauchy-type integral method and the synthetic, noise free G_{yy} data calculated by RTX using *ModelVision*. The average difference is 0.30 Eö.

with no terrain effects. Fig. 6 shows the simulated free-air G_{zz} response due to the bodies contaminated with 1 Eö/$\sqrt{\text{Hz}}$ (at 1 Hz) noise with terrain effect added. We applied Cauchy-type integral method and terrain corrected the free-air G_{zz} data for a 2.67 g cm^{-3} terrain density using a 10 m cell discretization of the merged LiDAR and SRTM DEMs to a square of 10 km side length centred about each station (Fig. 7). This resulted in the DEM being represented by approximately two million topographically conforming triangular cells. We observed how our result compare very well with the terrain corrected G_{zz} data for a 2.67 g cm^{-3} terrain density also provided by RTX (Fig. 8). Fig. 9 shows the difference between the 2.67 g cm^{-3} terrain corrected synthetic, contaminated with the noise G_{zz} data, calculated using the 3-D Cauchy-type integral method and the synthetic, noise free G_{zz} data calculated by RTX using ModelVision. As one would expect, we can see just a random noise in this data, which confirms the proper work of the developed terrain correction method. The root mean square difference between our 3-D Cauchy-type integral terrain correction and true G_{zz} response of the prisms is 0.34 Eö (Fig. 9), while the magnitude of G_{zz} field is on the order of 30 Eö.

Next, we consider the free-air G_{xx} data. Fig. 10 shows the noise-free G_{xx} response due to the bodies with no terrain effects. Fig. 11 shows the simulated free-air G_{xx} response due to the bodies contaminated with 1 Eö/$\sqrt{\text{Hz}}$ (at 1 Hz) noise with terrain effect added. We terrain corrected the free-air G_{xx} data for a 2.67 g cm^{-3} terrain density using a 10 m cell discretization of the merged LiDAR and SRTM DEMs as per the previous paragraph (Fig. 12). The root mean square difference between our 3-D Cauchy-type integral terrain correction and true G_{xx} response of the prisms is 0.35 Eö (Fig. 13), while the magnitude of G_{xx} field is on the order of 15 Eö.

Finally, we consider the free-air G_{yy} data. Fig. 14 shows the noise-free G_{yy} response due to the bodies with no terrain effects. Fig. 15 shows the simulated free-air G_{yy} response due to the bodies contaminated with 1 Eö/$\sqrt{\text{Hz}}$ (at 1 Hz) noise with terrain effect added. We terrain corrected the free-air G_{yy} data for a 2.67 g cm^{-3} terrain density using a 10 m cell discretization of the merged LiDAR and SRTM DEMs as described earlier (Fig. 16). The root mean square difference between our 3-D Cauchy-type integral terrain correction and true G_{yy} response of the prisms is 0.30 Eö (Fig. 17), while the magnitude of G_{yy} field is on the order of 15 Eö.

Differences between our terrain corrections and the true responses of the prisms can be attributed to noise and prism-based method by which the terrain response was calculated by RTX. In our current implementation of the software, each of the above terrain corrections for all 4687 stations and approximately two million triangular cells required 7 hr on a desktop PC running Windows 7 with a single 2.8 GHz processor with 8 GB RAM. This may be further optimized by increasing the discretization as a function of distance per standard practice with volume integral methods. We also note that the 3-D Cauchy-type integrals are linear, and thus lend themselves to large-scale parallelization. This is the subject of our ongoing software development. We note also that in practice,

the terrain response needs to be filtered prior to its subtraction from the free-air data, though this processing stage was not required for this particular model study.

6 DISCUSSION AND CONCLUSIONS

We have introduced a method of modelling the gravity field and its gradients based on the theory of Cauchy integral analogues that extends the principles of classic Cauchy integral theory to 3-D potential fields. In particular, we have demonstrated how we are able to calculate the gravity and gravity gradiometry responses of 3-D bodies as surface integrals over arbitrary volumes that may have spatially (i.e. vertical and horizontal) variable densities. This is particularly suited to the terrain (and bathymetric) correction of gravity and gravity gradiometry data that have a very large number of observation stations, have variable altitudes, and have DEMs produced from merged LiDAR and SRTM data.

Practically all existing methods of terrain corrections are based on the prismatic discretization and their associated volume integration. As discussed by Li & Chouteau (1998), a variety of closed form analytic forms exist for evaluating the volume integral of the gravity field for a right-rectangular prism

$$g_z(\mathbf{r}') = -G\rho_0 \int_{z_1}^{z_2}\int_{y_1}^{y_2}\int_{x_1}^{x_2} \frac{z-z'}{|\mathbf{r}-\mathbf{r}'|^3} dxdydz. \tag{62}$$

For example, Okabe (1979) derived the expression

$$g_z(\mathbf{r}') = -G\rho_0 \times \sum_{i=1}^{2}\sum_{j=1}^{2}\sum_{k=1}^{2} \mu_{ijk} x_i \left[\ln(y'_j + r_{ijk}) + y'_j \ln(x'_i + r_{ijk}) + 2z_k \arctan \frac{x'_i + y'_j + r_{ijk}}{z'_k} \right], \tag{63}$$

where $x'_i = x - x_i$, $y'_i = y - y_i$, $z'_i = z - z_i$, $r_{ijk} = \sqrt{(x'_i)^2 + (y'_i)^2 + (z'_i)^2}$ and $\mu_{ijk} = (-1)^i(-1)^j(-1)^k$. For every right-rectangular prism, eq. (63) requires the evaluation of 16 logarithms and 8 arctangents. For decades now, eq. (63) has been popularized in 3-D gravity inversion software (e.g. Li & Oldenburg 1998).

For Cauchy-type representation of a right-rectangular prism, one should calculate the surface integrals over the top of the prism and over the vertical sides of the prism. Note, however, that, for two neighboured prisms, the corresponding surface integrals over the sides of the prisms attached one to another would have the same values but opposite signs, identically cancelling each other. Therefore, the integration is required over the top of the prism. In the case of right-rectangular prisms, eq. (38) takes the form

$$g_\alpha\left(\mathbf{r}'_n\right) = \sum_{k=1}^{N_m} f_\alpha^{(nk)} h^{(k)}, \tag{64}$$

where:

$$f_\alpha^{(nk)} = -G\rho_0 \frac{\widetilde{r}_\alpha^{(k)} - r_\alpha^{(n)\prime}}{\left|\widetilde{\mathbf{r}}_k - \mathbf{r}'_n\right|^3} \Delta x \Delta y. \tag{65}$$

Compared to eq. (63), eq. (65) has a significantly lower computational complexity as it directly avoids the evaluation of 24 transcendental functions.

At the same time, it is well known that steep surfaces are difficult to describe by a combination of the rectangular prisms. One would need to use a very fine prismatic discretization to properly approximate a simple but steep surface. We avoid this limitation of the conventional methods by introducing 3-D Cauchy-type integrals and evaluating surface integrals numerically on a topographically conforming grid with a resolution equal to the DEM. This method avoids prismatic discretization of the DEMs and has lower computational complexity associated with volume integration as per standard practice. In addition, our method has a capability of including the vertically varying density models in the same Cauchy-type integral representations of the gravity and gravity gradient fields.

Ongoing research is focused on the use of Cauchy-type integral representations for the 3-D inversion of gravity and gravity gradiometry data.

ACKNOWLEDGEMENTS

The authors acknowledge TechnoImaging for support of this research, and permission to publish. Zhdanov and Liu acknowledge support of the University of Utah's Consortium for Electromagnetic Modeling and Inversion (CEMI). Rio Tinto Exploration Pty Ltd is acknowledged for providing the synthetic airborne gravity gradiometry data from the Kauring test site, and for permission to publish.

We are also thankful to Dr. Fernando Sanso and two anonymous reviewers for their valuable suggestions which helped to improve the paper.

REFERENCES

Bitsadze, A.V., 1953. Space analog of the Cauchy-type integral and some of its applications (in Russian), *Izv. Akad. Nauk SSSR Ser. Math.,* **17,** 525–538.

Bitsadze, A.V., 1972. *Fundamentals of Theory of Analytical Functions of a Complex Variable* (in Russian), Nauka, Moscow.

Davies, A.J., Foot, R., Joshi, G.C. & McKellar, B.H.J., 1989. Quaternionic methods in integral transforms of geophysical interest, *Geophys. J. Int.,* **99**(3), 579–582.

Davis, K., Kass, M.A. & Li, Y., 2011. Rapid gravity and gravity gradiometry terrain corrections via an adaptive quadtree mesh discretization, *Explor. Geophys.,* **42,** 88–97.

Dransfield, M. & Zeng, Y., 2009. Airborne gravity gradiometry: terrain corrections and elevation error, *Geophysics,* **74,** I37–I42.

Gakhov, F.D., 1997. *Boundary Value Problems* (in Russian), 3rd edn, Nauka, Moscow.

Grujic, M., 2012. Data processing requirements for an 1 Eö/$\sqrt{\text{Hz}}$ AGG system. *Presented at 22*nd *ASEG Conference and Exhibition,* Brisbane.

Hammer, P.T.C., Hildebrand, J.A. & Parker, R.L., 1991. Gravity inversion using seminorm minimization: density modeling of Jasper Seamount, *Geophysics,* **56,** 68–79.

Howard, D., Grujic, M. & Lane, R., 2010. The Kauring airborne gravity and airborne gravity gradiometer test site, Western Australia, in *Airborne Gravity 2010 – Abstracts from the ASEG-PESA Airborne Gravity 2010 Workshop,* pp. 107–114, ed. Lane, R.J.L., Geoscience Australia Record 2010/23, Sydney.

Hwang, C., Wang, C. & Hsiao, Y., 2003. Terrain correction computation using Gaussian quadrature, *Comput. Geosci.,* **29,** 1259–1268.

Jekeli, C. & Zhu, L., 2006. Comparison of methods to model the gravitational gradients from topographic data bases, *Geophys. J. Int.,* **166,** 999–1014.

Kass, M.A. & Li, Y., 2008. Practical aspects of terrain correction in airborne gravity gradiometry surveys, *Explor. Geophys.,* **39,** 198–203.

Kirby, J. & Featherstone, W., 2002. High-resolution grids of gravimetric terrain correction and complete Bouguer corrections over Australia, *Explor. Geophys.,* **33,** 161–165.

Lane, R., 2004. Integrating ground and airborne data into regional gravity compilations, in *Airborne Gravity 2004 – Abstracts from the ASEG-PESA Airborne Gravity 2004 Workshop,* pp. 81–97, ed. Lane, R., Geoscience Australia Record 2004/18, Sydney.

Li, X. & Chouteau, M., 1998. Three-dimensional gravity modeling in all space, *Surv. Geophys.,* **19,** 339–368.
Li, Y. & Oldenburg, D.W., 1998. 3D inversion of gravity data, *Geophysics,* **63,** 109–119.
Moisil, G.C. & Theodoresco, N., 1931. Functions holomorphes dans l'espace, *Mathematica,* **5,** 142–153.
Murphy, C.A., 2010. Recent developments with Air-FTG, in *Airborne Gravity 2010 – Abstracts from the ASEG-PESA Airborne Gravity 2010 Workshop,* pp. 142–151, ed. Lane, R., Geoscience Australia Record 2010/23, Sydney.
Okabe, M., 1979. Analytical expressions for gravity anomalies due to homogeneous polyhedral bodies and translations into magnetic anomalies, *Geophysics,* **64,** 730–741.
Parker, R.L., 1973. The rapid calculation of potential anomalies, *Geophys. J. R. astr. Soc.,* **31,** 447–455.
Parker, R.L., Shure, L. & Hildebrand, J.A., 1987, The application of inverse theory to seamount magnetism, *Rev. Geophys.,* **25,** 17–40.
Parker, R.L., 1995. Improved Fourier terrain correction, Part I, *Geophysics,* **60,** 1007–1017.
Parker, R.L., 1996. Improved Fourier terrain correction, Part II, *Geophysics,* **61,** 365–372.
Zhdanov, M.S., 1973. Properties of the gravitational potential of a three-dimensional homogeneous body (in Russian), *Geol. Geophys.,* **12,** 96–101.
Zhdanov, M.S., 1974. Theory of intepretation of gravitational anomalies determined by three space coordinates (in Russian), *Izv. Akad. Nauk SSSR Fiz. Zem.,* **9,** 32–46.
Zhdanov, M.S., 1975. The gravitational field of a three-dimensional layered medium (in Russian), *Geol. Geophys.,* **6,** 112–120.
Zhdanov, M.S., 1980. Use of Cauchy integral analogs in the geopotential field theory, *Ann. Geophys.,* **36,** 447–458.
Zhdanov, M.S., 1984. *Cauchy Integral Analogs in Geophysical Field Theory* (in Russian), Nauka, Moscow.
Zhdanov, M.S., 1988. *Integral Transforms in Geophysics,* Springer-Verlag, Berlin.
Zhou, X., 2008. 2D vector gravity potential and line integrals for the gravity anomaly caused by a 2D mass of depth-dependent density contrast, *Geophysics,* **73,** I43–I50.
Zhou, X., 2009. 3D vector gravity potential and line integrals for the gravity anomaly of a rectangular prism with 3D variable density contrast, *Geophysics,* **74,** I43–I53.

APPENDIX A: 3-D ANALOGUE OF THE POMPEI FORMULA

The Pompei formula can be derived based on Gauss theorem:

$$\iiint_D (\nabla \cdot \Phi)\ dv = \iint_S \Phi \cdot \mathbf{n}\, \mathrm{d}s, \tag{A1}$$

where $\Phi(\mathbf{r})$ is a vector function continuously differentiable everywhere in the domain D; $\mathbf{n}$ is a unit vector of the normal to S directed outside the domain D, bounded by the surface S.

Let us introduce a potential field, $\mathbf{F}(\mathbf{r})$, defined within a domain, D, and satisfying the equations:

$$\nabla \times \mathbf{F} = 0,\ \nabla \cdot \mathbf{F} = q, \quad \mathbf{r} \in D. \tag{A2}$$

We also consider a fundamental Green's function for the Laplace equation,

$$P(\mathbf{r}) = -1/4\pi|\mathbf{r} - \mathbf{r}'|. \tag{A3}$$

To derive a 3-D Pompei formula, we represent the vector function $\Phi(\mathbf{r})$ in the form

$$\Phi(\mathbf{r}) = (\mathbf{C} \cdot \mathbf{F}(\mathbf{r}))\, \nabla P(\mathbf{r}) + \nabla P(\mathbf{r}) \times [\mathbf{F}(\mathbf{r}) \times \mathbf{C}], \tag{A4}$$

where $\mathbf{C}$ is arbitrary constant vector. Straight forward calculations show that

$$\nabla \cdot \Phi = \mathbf{C} \cdot \left[\nabla^2 P\, \mathbf{F} + (\nabla \cdot \mathbf{F})\ \nabla P\right],$$

$$\Phi \cdot \mathbf{n} = \mathbf{C} \cdot \{(\mathbf{n} \cdot \mathbf{F})\nabla P + [\mathbf{n} \times \mathbf{F}(\mathbf{r})] \times \nabla P\}.$$

Applying the Gauss theorem to the vector function $\Phi(\mathbf{r})$ and taking into consideration that the vector $\mathbf{C}$ is arbitrary, we arrive at the following corollary of the Gauss theorem

$$\iiint_D \left[\nabla^2 P\, \mathbf{F} + (\nabla \cdot \mathbf{F})\ \nabla P\right] \mathrm{d}v = \iint_S \{(\mathbf{n} \cdot \mathbf{F})\nabla P + [\mathbf{n} \times \mathbf{F}(\mathbf{r})] \times \nabla P\}\ ds. \tag{A5}$$

The fundamental Green's function satisfies to the equation:

$$\nabla^2 P\ = \delta\left(\mathbf{r} - \mathbf{r}'\right), \tag{A6}$$

where $\delta(\mathbf{r} - \mathbf{r}')$ is the singular Dirac delta-function.

Substituting eqs (A3) and (A6) into expression (A5), after some algebra, we obtain the following integral formula:

$$-\frac{1}{4\pi}\iint_S \left\{(\mathbf{n} \cdot \mathbf{F})\nabla\frac{1}{|\mathbf{r} - \mathbf{r}'|} + [\mathbf{n} \times \mathbf{F}(\mathbf{r})] \times \nabla\frac{1}{|\mathbf{r} - \mathbf{r}'|}\right\} \mathrm{d}s + \frac{1}{4\pi}\iiint_D (\nabla \cdot \mathbf{F})\ \nabla\frac{\mathbf{1}}{|\mathbf{r} - \mathbf{r}'|}\, dv = \begin{cases} \mathbf{F}(\mathbf{r}'), & \mathbf{r}' \in D \\ \mathbf{0}, & \mathbf{r}' \in CD \end{cases}. \tag{A7}$$

According to the definition (see eq. 1), the surface integral in eq. (A7) is nothing else but the 3-D Cauchy-type integral $\mathbf{C}^S(\mathbf{r}', \mathbf{F})$.

Thus, we have arrived at the 3-D analogue of the Pompei formula

$$\mathbf{C}^S\left(\mathbf{r}', \mathbf{F}\right) + \frac{1}{4\pi}\iiint_D (\nabla \cdot \mathbf{F})\nabla\frac{1}{|\mathbf{r} - \mathbf{r}'|}dv = \begin{cases} \mathbf{F}(\mathbf{r}'), & \mathbf{r}' \in D \\ \mathbf{0}, & \mathbf{r}' \in CD \end{cases}. \tag{A8}$$

APPENDIX B: MATRIX FORM OF THE CAUCHY-TYPE INTEGRAL

It is convenient to express 3-D Cauchy integrals in matrix notations. This matrix representation is based on the fact that many operations of vector algebra can be written using operations on the scalar components of the corresponding matrices, reproducing the scalar components of the vectors in some Cartesian coordinates with the basis $\{\mathbf{d}_x, \mathbf{d}_y, \mathbf{d}_z\}$. For example, the dot product of two vectors,

$$\mathbf{a} = a_x\mathbf{d}_x + a_y\mathbf{d}_y + a_z\mathbf{d}_z \text{ and } \mathbf{b} = b_x\mathbf{d}_x + b_y\mathbf{d}_y + b_z\mathbf{d}_z,$$

is

$$\mathbf{a} \cdot \mathbf{b} = a_x b_x + a_y b_y + a_z b_z = a_\alpha b_\beta \delta_{\alpha\beta},\ \alpha, \beta = x, y, z, \tag{B1}$$

where we use the symmetric Kronecker symbol, $\delta_{\alpha\beta}$, defined by eq. (8). Note that, in eq. (B1) and everywhere throughout this paper, we use an agreement on summation that the twice recurring index indicates the summation over this index, for example,

$$a_\alpha b_\beta \delta_{\alpha\beta} = \sum_{\alpha=x,y,z}\ \sum_{\beta=x,y,z} a_\alpha b_\beta \delta_{\alpha\beta}. \tag{B2}$$

Similarly, the vector product of two vectors can be expressed using the skew-symmetric Kronecker symbol, $\varepsilon_{\alpha\beta\xi}$,

$$\mathbf{a} \times \mathbf{b} = a_\alpha b_\beta \varepsilon_{\alpha\beta\xi} \mathbf{d}_\xi, \ \alpha, \beta, \xi = x, y, z, \tag{B3}$$

where ε-symbol is antisymmetric with respect to any two indices, and it is equal to 1 for noncoincident indices,

$$\varepsilon_{\alpha\beta\xi} = -\varepsilon_{\beta\alpha\xi} = 1, \ \text{if} \ \alpha \neq \beta \neq \xi,$$

and equal to zero if any two indices happen to coincide, for example,

$$\varepsilon_{xxy} = 0.$$

We should note also that there exists a simple relationship between the Kronecker δ- and ε-symbols

$$\varepsilon_{\alpha\zeta\eta} \ \varepsilon_{\beta\xi\zeta} = \delta_{\alpha\xi}\delta_{\beta\eta} - \delta_{\alpha\beta}\delta_{\xi\eta}. \tag{B4}$$

We can write the triple vector product of the vectors **a**, **b** and **c**, using formula (B3), as follows

$$\mathbf{a} \times [\mathbf{b} \times \mathbf{c}] = a_\alpha \ b_\beta \ c_\xi \varepsilon_{\alpha\zeta\eta} \ \varepsilon_{\beta\xi\zeta} \mathbf{d}_\eta. \tag{B5}$$

We can derive now matrix form of the Cauchy-type integral using formulas (B1), (B3) and (B5). Indeed, eq. (6) provides representations of the vectors $\mathbf{C}^S$, φ, **n** and $\nabla \frac{1}{|\mathbf{r}-\mathbf{r}'|}$ via their scalar components in Cartesian basis $\{\mathbf{d}_x, \mathbf{d}_y, \mathbf{d}_z\}$. Substituting eq. (6) in the integrand of expression (1) for the 3-D Cauchy-type integral, and taking into account formulas (B1), (B3) and (B5), we can write

$$\begin{aligned}
&(\mathbf{n} \cdot \varphi) \nabla \frac{1}{|\mathbf{r} - \mathbf{r}'|} + (\mathbf{n} \times \varphi) \times \nabla \frac{1}{|\mathbf{r} - \mathbf{r}'|} \\
&\quad = \left(\delta_{\alpha\eta}\delta_{\beta\xi} + \varepsilon_{\alpha\eta\zeta} \ \varepsilon_{\beta\xi\zeta}\right) \varphi_\beta \frac{r_\eta - r'_\eta}{|\mathbf{r} - \mathbf{r}'|^3} n_\xi \mathbf{d}_\alpha \\
&\quad = \Delta_{\alpha\beta\xi\eta} \varphi_\beta \frac{r_\eta - r'_\eta}{|\mathbf{r} - \mathbf{r}'|^3} n_\xi \mathbf{d}_\alpha,
\end{aligned} \tag{B6}$$

where the four-index Δ-symbol is expressed in the terms of the Kronecker δ- and ε-symbols, or, with due account of (B4), in terms of the symmetric δ-symbol only:

$$\Delta_{\alpha\beta\xi\eta} = \delta_{\alpha\eta}\delta_{\beta\xi} + \varepsilon_{\alpha\eta\zeta} \ \varepsilon_{\beta\xi\zeta} = \delta_{\alpha\beta}\delta_{\xi\eta} + \delta_{\alpha\eta}\delta_{\beta\xi} - \delta_{\alpha\xi}\delta_{\beta\eta}. \tag{B7}$$

Substituting expression (B6) into eq. (1), we arrive at the matrix form of the Cauchy-type integral

$$C^S_\alpha \left(\mathbf{r}', \varphi\right) = -\frac{1}{4\pi} \iint_S \Delta_{\alpha\beta\xi\eta} \varphi_\beta \frac{r_\eta - r'_\eta}{|\mathbf{r} - \mathbf{r}'|^3} n_\xi ds,$$

$$\alpha, \beta, \xi, \eta = x, y, z. \tag{B8}$$